UNIVERSITY OF CALIFORNIA
RIVERSIDE

Electrospun Pristine and Composited Polyvinylidene Fluoride (PVDF) Fiber Mats as Energy Harvester and Antimicrobial Mask

A Thesis submitted in partial satisfaction
of the requirements for the degree of

Master of Science

in

Chemical and Environmental Engineering

by

Yun Young Choi

September 2021

Thesis Committee:
Dr. Xin Ge, Chairperson
Dr. Jin Nam
Dr. Juchen Guo

The Thesis of Yun Young Choi is approved:

_____

_____

_____

Committee Chairperson

University of California, Riverside

Acknowledgments

Joining Dr. Nosang Myung's lab was one of the best things that I have done. This lab has taught me so many things and helped me see things in different perspective. I am ever so grateful for the kindness, care, and guidance that Dr. Myung has shown me. Thank you for this opportunity and lessons that I have learned during my time at UCR. I will have much to learn but I am where I am currently thanks to Dr. Myung.

I am grateful of all the relationships that I have made during my time in this lab, but I am especially thankful to have met and been under Sooyoun Yu when she was a Ph.D. student in Dr. Myung's lab. Thank you for your patience and guidance when I was confused and lost. I hope to be more like you and hope that I also can help others the ways you have helped me.

Special thanks to my parents, family, and friends for all the support that they have shown me for it was not an easy time for all of us. I was able to laugh and make my time at UCR memorable thanks to all. Thank you for pushing me forward and encouraging me in everyone's unique ways.

Lastly, my work could not have been possible without funding from National Science Foundation, Division of Chemical, Bioengineering, Environmental, and Transport System (CBET) (Fund number 2030571).

ABSTRACT OF THESIS

Electrospun Pristine and Composited Polyvinylidene Fluoride (PVDF) Fiber Mats as Energy Harvester and Antimicrobial Mask

by

Yun Young Choi

Master of Science, Graduate Program in Chemical and Environmental Engineering
University of California, Riverside. September 2021
Dr. Xin Ge, Chairperson

Piezoelectric polymer, which can generate electricity under mechanical strain, have many different applications in medical field, energy generation and harvesting and most recently, as an air filter for face mask. With the global pandemic, the demand for personal protective equipment (PPE) such as face masks is higher than ever. N95 masks are considered the gold standard PPE against the viral pathogens and have thus suffered a shortage many times throughout the pandemic. In addition, the electrostatic charge inserted into the melt-blown polypropylene fiber-based mask material to capture bacterial and viral particles is easily removed during the disinfection process, allowing for only single use. Thus, creative solutions to enhance the reusability while exhibiting comparable protection efficiency to the N95 masks are highly desirable.

Though polyvinylidene fluoride tetrafluoroethylene (PVDF-TrFE) has so far exhibited the highest piezoelectric charge constants, its high cost deems it unsuitable for industry-scale production. The cost effective PVDF with lower piezoelectric properties

was thus chosen as the host polymer. Electrospinning not only is a simple, cost-effective, scalable method to fabricate polymer nanofibers, but also allows for fine tuning of process conditions, enabling precise control of nanofiber properties such as morphology, which has recently been shown to significantly affect piezoelectric properties.

The overarching goal of this project is to fabricate multifunctional composite nanofibers with air filtration and antimicrobial capabilities enabled by piezoelectric effect. Diameter of PVDF nanofibers with various antimicrobial additives (e.g., silver) function was optimized via process control of electrospinning. Additionally, antimicrobial, percent removal, filter efficiency and pressure drop testing were conducted to compare electrospun PVDF nanofibers with current N95 mask. During the preliminary results, Silver Nanoparticles embedded PVDF nanofiber exhibited great potential to be used as a multifunctional, longer lasting, and easier to breathe face mask filter.

TABLE OF CONTENTS

LIST OF FIGURES

LIST OF TABLES

1. Enhancement of Piezoelectric Properties of Polyvinylidene fluoride Nanofibers by Electrospinning and Post Thermal Treatment

1.1 Abstract

Pristine nanofibers based on Polyvinylidene fluoride (PVDF) were electrospun with solution conditions systematically varied through series of design of experiments (DOE). DOE analyses revealed the effect of the operating conditions on resulting nanofiber properties including physical and piezoelectrical properties. PVDF concentration by wt.% and the molecular weight of the solution was the predominant factor for solution viscosity which controlled the nanofiber dimensions such as average fiber diameters and fiber fraction. These electrospun PVDF nanofibers went through post thermal treatment to further enhance the piezoelectric properties. Size and temperature-dependent piezoelectric properties and voltage output were studied and compared to material characterizations by Fourier-transform infrared (FT-IR) spectroscopy and X-ray diffraction (XRD).

1.2 Introduction

1.2.1 Nanofiber Synthesis

Polymeric nanofiber has been widely known and used for their high surface area to volume ratio, variety of polymer choices, highly porous structure, and flexibility. Depending on their properties, polymeric nanofibers can be suitable for a wide range of

applications such as drug delivery, cosmetics, tissue engineering, filtration system and energy harvesting and generation.

Methods of synthesizing nanofibers include self-assembly[1,2], thermal induced phase separation[3], electrospinning[4,5], solution blowing[6], drawing techniques[7–9], template synthesis[10,11] and centrifugal spinning[12]. Table 1.1 shows overview of different nanofiber synthesis methods. Among these methods, electrospinning is widely chosen because it not only is simple and cost-effective, but also allows for control of nanofiber properties such as the fiber diameter via fine-tuning of its working conditions. In addition, properties of electrospun nanofibers can be further optimized by post-electrospinning processes including thermal, electrochemical, and chemical treatments. The process of electrospinning is driven by a high voltage applied to a small droplet of solution, which becomes charged until a large enough electrostatic repulsion is formed that its surface tension is overcome and is stretched into a jet of nanofibers. When the stream of the solution erupts, the point of eruption is pulled into a cone shape, known as the Taylor cone. As the droplet continues to be pulled, the solvent evaporates and the charges migrate to the surface and the generated nanofibers are collected onto the grounded collector.[13]

Table 1.1 Summary of nanofiber synthesis methods

Method	Principle	Advantages	Disadvantages	Ref.
Self-assembly	Formation of fibrous synthesis that forms matrix of gel via non-covalent interactions	Works with biomolecules	Long time, low stability	1,2
Thermal induced phase separations	Melt blending polymer, cast into shape and removal of dilutant	Good biocompatibility, control of pore phases	Low tensile strength, limited flexibility, depends on crystallization temperature	3
Electrospinning	High electric field charges and pulls precursor solution into jet of nanofibers	Simple, cost-effective; virtually no limit on materials; scalable	High voltage; organic solvents	4,5
Solution blowing	Solution pumped through nozzle, high gas velocity flow onto collector	High production rate	High pressure gas	6
Drawing techniques	Pulling of nanofiber from polymer droplets.	Production of single nanofibers	Depends on the orifice size, limited fiber diameter (100nm),	7-10
Template synthesis	Chemical and physical methods of etching and calcination and deposition along template	Uniform dimensions	Catalyst required, cannot craft continuous fibers	11
Centrifugal spinning	Spinning fluid placed in rotating spinning head, nanofiber ejected by centrifugal force overcoming surface tension	High speed, low cost	High temperature, disordered nanofibers	12

There are many different nanofiber applications such as in biomedical field as a replication of collagen fibrils to act as a barrier for burn wounds[14], as well as for drug delivery, tissue repair and generations. There is also researches going on to use heat transfer from nanofibers to be used as a chemical and biological protection barrier[15]. Nanofiber application has also been used as water[16,17] and air filtration[18] sheet and energy storage and harvesting storage devices[19]. Application in area of energy harvesting and generation are heavily investigated to eventually replace the over usage of fossil fuels. Fossil fuels are convenient but has many drawbacks such as being a limited resource, and greenhouse gas emission that leads to smog, pollution, food supply disruption, increase of wildfires that affects all human beings. Some alternative energy sources include solar, wind, hydro energy. These uses thermoelectric and nanogenerators that uses thermal gradient and motion as the source of energy production, respectively. These have ambient and natural sources, making these energy sources sustainable. Of this nanogenerator, there are piezoelectric materials that can be used for many versatile forms in energy harvesting and generation.

1.2.2 Piezoelectricity

Piezoelectricity refers to an electromechanical coupling factor that allows for direct conversion from mechanical to electrical energy, also known as the direct piezoelectric effect. The indirect piezoelectric effect is the conversion of electrical energy to a mechanical response. Piezoelectricity was discovered in 1880 by Pierre Currie and Paul Jacques who proved that some materials such as quartz that have asymmetrical structure would give out electrical potential when mechanical stress is applied.

The usage of piezoelectricity in different applications has been emerging more recently in medical[20], consumer electronics, sensors, and energy harvesting[21]. The two major type of piezoelectric materials that are used are ceramics and polymers. While ceramics have high piezoelectric charge constant, a value typically utilized to evaluate piezoelectric properties of a material, they are not suitable for some energy harvesting applications due to their brittle nature. In addition, some ceramics like lead zirconate titanate (PZT) contain lead, which is toxic and thus limits the applications for piezoelectric ceramics where biocompatibility is required. Polymers, on the other hand, exhibit relatively inferior piezoelectric properties, but their flexibility and biocompatibility widen their range of potential applications. Of the piezoelectric polymers, polyvinylidene fluoride (PVDF) exhibits one of the highest piezoelectric constants. PVDF exists in several phases including the α-, β-, γ- phases[22]. PVDF at room temperature exists in a non-polar phase with fluorine atoms distributed evenly on either side of the polymer chain (TGTG'), also known as an α-phase. The β-phase (TTTT) consists of fluorine atoms only on one side of the polymer chain and is known as the electroactive phase that shows the most piezoelectric properties. The γ-phase (TTTGTTTG') contains some fluorine atoms on one side of the chain but it is not as strong as the β-phase.

The key to enhancing the piezoelectric properties of PVDF is to increase the proportion of the β-phase, also known as the electroactive phase. Typically, in PVDF films, post-synthesis mechanical stretching and electrical poling were required to induce the β-phase. Electrospinning, on the other hand, can provide these processes *in-situ* due

to the high electric field applied during electrospinning[23–25]. PVDF, which exist in semi-crystalline , with electrospinning conditions as well as solution parameters and environmental conditions strongly affect not only the fiber morphology but also the phase of PVDF.[26,27] Yee et al. also states that the high voltage or high stretching ratio of the jets applied during electrospinning also benefits the crystallization of β-phase, as well as the alignment of the fibers onto the drum collector.[28] Another way to promote the formation of the electroactive phase in PVDF is by making α-phase less energetically stable. PVDF copolymers created with monomers such as tetrafluoroethylene (TFE) or trifluoroethylene (TrFE) and these monomers will create energetically favorable molecular chain with electroactive phases. With these alterations, PVDF-TrFE will have more active β-phase without mechanical orientation.

Post thermal treatment can also increase the β-phase content of PVDF. This simple method leads to a change in the structural characteristics such as crystallinity and polymer chain alignments[29]. Gregorio et al. investigated the temperature-dependent phase change in PVDF and found that at temperatures lower than 70 °C, β-phase was predominantly present, α- and β-phase between 70 and 110 °C, and α-phase above 110°C.[30]

Electrospinning has a wide range of conditions that can affect the resulting nanofiber properties and in order to fine tune these conditions to tailor the nanofiber properties for specific application, there need to be a comprehensive understanding about which conditions are effective in controlling certain nanofiber properties and effect of such conditions and this can be done by using design of experiment (DOE). DOE is a

systematic variation of factors to quantitatively determine the effect of solutions conditions on electrospun solution's nanofiber morphology and with this system, the maximum amount of information can be obtained from minimum experiments. Yu et al. have demonstrated usage of DOE in controlling PAN fiber diameter for electrochemical application.[31] Following DOE, the effect of operation conditions in electrospinning PVDF based composite nanofibers on morphology and piezoelectric properties have been studied. This section will focus on the size and temperature dependent piezoelectric properties of electrospun PVDF nanofibers. These piezoelectric electrospun nanofibers have many versatile applications such as piezocatalyst, biological applications, physical sensors, energy harvesting and even as air filtration system. Nanofiber properties such as fiber diameter and fiber fraction were analyzed as a function of solution condition based on a series of DOE. Material characterization by Fourier-transform infrared (FT-IR) spectroscopy and X-ray diffraction (XRD) were performed and their results were correlated with the piezoelectric properties characterizations obtained by cantilever and piezoelectric force microscopy (PFM).

1.3 Materials and Methods

1.3.1 Materials

Polyvinylidene fluoride (PVDF, MW=180,000 and 534,000 g/mol), pyridine, and formic acid were purchased from Sigma Aldrich. N,N-dimethylformamide (DMF) and Acetone were purchased from Fisher Scientific. All materials were used without further treatment or purification.

1.3.2 Solution preparation

Electrospinning solutions were prepared by mixing various amounts of PVDF in 64:36 DMF/acetone (by vol.). PVDF was mixed with DMF first then vigorously stirred at approximately 70 ^{o}C until homogeneous. Once the solution was cooled to room temperature, acetone was added and then stirred until homogenous. Pyridinium formate (PF) was obtained by mixing equimolar amounts of pyridine and formic acid and then was added to the PVDF solution to increase the electrical conductivity. All solutions were allowed to reach room temperature before continuing onto the next step.

1.3.3 Solution characterization

Solution viscosity was measured using a viscometer (Brookfield DV-I Prime and DV2THB) and electrical conductivity using a glass-body electrical conductivity probe (K= 1.0, Apera Instruments) paired with an embedded conductivity circuit (Atlas Scientific, EZO-EC^{TM}) and an Arduino Uno Rev3 board. All solution properties measurements were taken at room temperature immediately before electrospinning to correlate them most closely to resulting nanofiber properties.

1.3.4 Electrospinning

The prepared PVDF solutions were drawn into a 5-mL BD Luer Lok syringe with a 25 or 20-guage needle, which was then loaded onto a syringe pump (New Era, NE-100). The needle tip was set at 10 cm from the drum collector. Negatively charged 16.5 kV was applied to the needle tip. The grounded drum collector was wrapped with aluminum foil and rotating at 400 rpm. Environmental conditions were kept constant at temperature of 23 °C and absolute humidity of 0.005kg water/kg dry air.

To investigate the effect of temperature on piezoelectric properties of PVDF nanofibers, the as-spun nanofiber samples were annealed in a box furnace (Thermo Scientific Thermolyne F47925-80 Muffle Furnace) at temperatures varying from 40 to 130° C for 2h in air.

1.3.5 Nanofiber properties characterization

1.3.5.1 Physical properties

Morphology of the nanofiber samples was observed with a scanning electron microscope (SEM, Fisher Scientific Prisma E). Obtained SEM images were imported to ImageJ software to measure the average fiber diameter, which was obtained by measuring the length of 30 unique nanofibers. Bead density was calculated by dividing the total number of beads from a single SEM image by the total area of the image. Fiber fraction was determined by the proportion of nanofibers in the total product, which could include beads and clumps. The molecular and crystal structure were observed with Fourier-transform infrared spectroscopy (FTIR, Perkin Elmer Frontier) and X-ray diffraction (XRD, Bruker D8 Discover), respectively. FTIR spectra were obtained by scanning from 400 to 4000 cm^{-1} at a resolution and scan increment of 2 and 0.5 cm^{-1}, respectively. Sample purity and phase analysis were evaluated using X-ray diffraction performed at room temperature using an in-house Bruker D8 Discover at $\lambda = 1.5406$ Å. Data was collected over the range of 10° - 60° in scattering angle (2θ) with a step size of 0.024°.

1.3.5.2 Piezoelectric properties

Electrodes based on aligned PVDF nanofibers were prepared to measure piezoelectric voltage output (V_3). PVDF nanofibers were electrospun onto a thin strip of aluminum foil wrapped tightly around a disc collector with diameter of 13 cm and width of 2.5 cm. This disc was then immobilized onto a metal rod at its center and then loaded onto lathe (Central Machinery 93799). The rotation of lathe was set approximately at 2000 rpm to align nanofibers collected on the foil. Negatively charged 17.5 kV voltage was applied to the needle tip, while positive 1kV voltage was applied to the collector[32]. As-spun PVDF nanofibers were cut into 4 x 1.2 cm^2 strip. A 7.2 x 1.6 x 0.01 cm^3 brass substrate covered on both sides with polyimide tape was prepared as the cantilever. Nanofiber sample was fixed to the center of the cantilever with double-sided copper tape on one side and the other side was insulated with polyimide tape. Two 24-gauge wires were soldered to outer part of the brass plate and then sealed with polyimide tape, which was connected to a breadboard with inputs to oscilloscope (Pico Technology, PicoScope 2000) to measure the output voltage from the nanofiber mat.

To measure the piezoelectric constants of individual fibers, PVDF nanofibers were sparsely collected on a gold sputtered silicon (Si) substrate during electrospinning. Atomic force microscope (AFM, Asylum Research MFP-3D) in tapping mode was used to visualize and locate a single fiber. The AFM mode was then switched to piezoelectric force microscopy (PFM) mode, where single point measurements were taken by applying alternating step voltage to AFM cantilever (Olympus AC2420TM). The piezoelectric

charge constant (d_{33}) was then calculated using the piezoelectric response from PFM using the following equation:

$$d_{33} = \frac{A]}{VQ} f \qquad \text{(Equation 1)}$$

Where A is the amplitude response, V is applied voltage (set at 3 V), Q is the quality factor of the AFM cantilever, and f is the correctional factor taken from the PPLN standard.

1.4 Results and Discussion

1.4.1 Fabrication of PVDF nanofibers

For better understanding of correlation between electromechanical and mechanical properties of PVDF nanofibers as a function of fiber dimensions, design of experiments (DOEs) was used to find optimal solution conditions to produce smooth nanofibers with controlled dimensions and minimum defects such as beads and clumps. Two factors, PVDF and PF concentration, were first tested, as the polymer concentration is typically known to control the solution viscosity, which has significant impact on nanofiber diameter, while the addition of PF was hypothesized to increase the solution electrical conductivity, which could enhance the spinnability of PVDF nanofibers. Increased electrical conductivity increased the conductivity of the solution and this will lead to better stretching of the fiber which results in better formation of smooth fibers. Based on this DOE, a total of 5 solutions were electrospun, and the resulting nanofibers were analyzed focusing on fiber fraction and fiber diameter.

		Solution conditions		Solution Properties		Fiber Properties		
Sample	Code	PVDF wt.%	PF Concentration [wt.%]	Viscosity [cP]	Electrical Conductivity [µS/cm]	Average fiber diameter [nm]	Fiber fraction [$\mu m^2/\mu m^2$]	Bead density [beads/μm^2]
1.1	(- -)	8	0.5	17.2	39.24	87 ± 25	0.39	0.61
1.2	(- +)	8	8.8	21.2	1363	90 ± 17	0.43	0.57
1.3	(0 0)	11	3	38.6	176.1	105 ± 31	0.51	0.49
1.4	(+ -)	14	0.5	59.9	65.17	89 ± 24	0.72	0.28
1.5	(+ +)	14	8.8	75.1	425.6	99± 27	0.69	0.31

Table 1.2 Design of experiment matrix varying PVDF and PF concentrations each with respective low (-) and high (+) values and their resulting solution properties.

From this run, it was shown that increasing the concentration of PVDF increased the viscosity of the solution which also correlated to increase in average fiber diameter measured. The viscosity of the solution went from 17.2 cP at 8 wt.% PVDF to 38.6 cP at 11 wt.% and 59.9 cP at 14 wt.% PVDF. This data supported that increasing the PVDF concentration corresponded to increase in the solution viscosity. This was an expected trend for other electrospun nanofiber such as PAN[31]. Increase of PF solution concentration also increased in electrical conductivity of the solution which showed increase in fiber fraction and decrease of defects such as beads and clumps up to certain concentration. As the electrical conductivity increased from 0.5 wt.% to 8.8 wt.%, the electrical conductivity of 8 wt.% PVDF went from 39.24 to 1363 µS/cm. And the bead density did decrease from 0.61 to 0.57 beads/μm^2. This trend was also seen at higher concentration of PVDF. Despite the increased fiber fraction, the SEM images in Figure 1.1a-e still show lots of impurities such as beads and clumps. DOE analysis was conducted from the results, and it can be seen in Figure 1.1f, that increasing the PVDF

concentration significantly increased the viscosity. The PF concentration and combination of PVDF and PF concentration also had positive impact on the viscosity, but it can be concluded that PVDF concentration has the biggest impact in change of viscosity. Figure 1.1g, shows DOE analysis of effect on electrical conductivity as the PVDF and PF concentration increases, and it can be seen that increasing PF concentration had positive impact on electrical conductivity while increasing PVDF concentration lowered electrical conductivity. From these results, it can be concluded that PVDF concentration predominantly effect viscosity while PF concentration predominantly effect electrical conductivity. Figure 1.1h shows that increasing the PVDF concentration had effect on increased fiber diameter. Figure 1.1i shows that the fiber fraction did increase as the PVDF concentration went up, but PF concentration did not have much effect on increasing the fiber fraction. This could be because the PVDF concentration from DOE 1 was too low that there were not enough nanofibers formed in the first place for PF solution to positively impact fiber fraction. After seeing that 14 wt.% PVDF solution had more beads and clumps compared to the amount of fibers present from the SEM image, literature survey was done to find a better range for PVDF concentrations. From the literature survey, the desired range of PVDF concentration was between 15 and 30 wt.%. So, this was set as the range for DOE 2 and from DOE 1, it was seen that increase in PF solution concentration did not proportionally decrease the number of defects of electrospun PVDF nanofibers. PF solutions were kept at 0.5 wt.% for all proceeding solutions to help increase electrical conductivity which helped increase fiber fraction and decrease defects seen. These results collectively indicated that both PVDF and PF

solution concentration had to be addressed to yield desired fiber fraction and fiber diameter.

Based on these observations, second DOE was designed to further increase the fiber fraction and decrease bead density. The low (-) value for PVDF for this DOE was previous DOE's high value (+) of 14 wt.% . PF solution was kept at 0.5 wt.% for both lower and upper limit. For this DOE, Mw were altered. Previous DOE had low fiber fraction and high bead density. After intensive literature survey[23,33,34], electrospun PVDF concentrations were targeted between 14 wt.% and 20 wt.% as PVDF concentration of 25 wt.% yielded a solution too viscous to electrospin and became gel-like which was also seen during literature survey for higher PVDF concentrations[35]. . Molecular weight of PVDF was altered between 180,000 in a pellet form and 534,000 in a powdered form. From Table 1.3, it can be seen that at the same PVDF concentration, increasing the MW of the PVDF polymer have drastic effect on the viscosity of the solution. The viscosity went from 59.9 to 275.9 cP for 14 wt.% PVDF and same trend was seen for higher PVDF concentration as well.

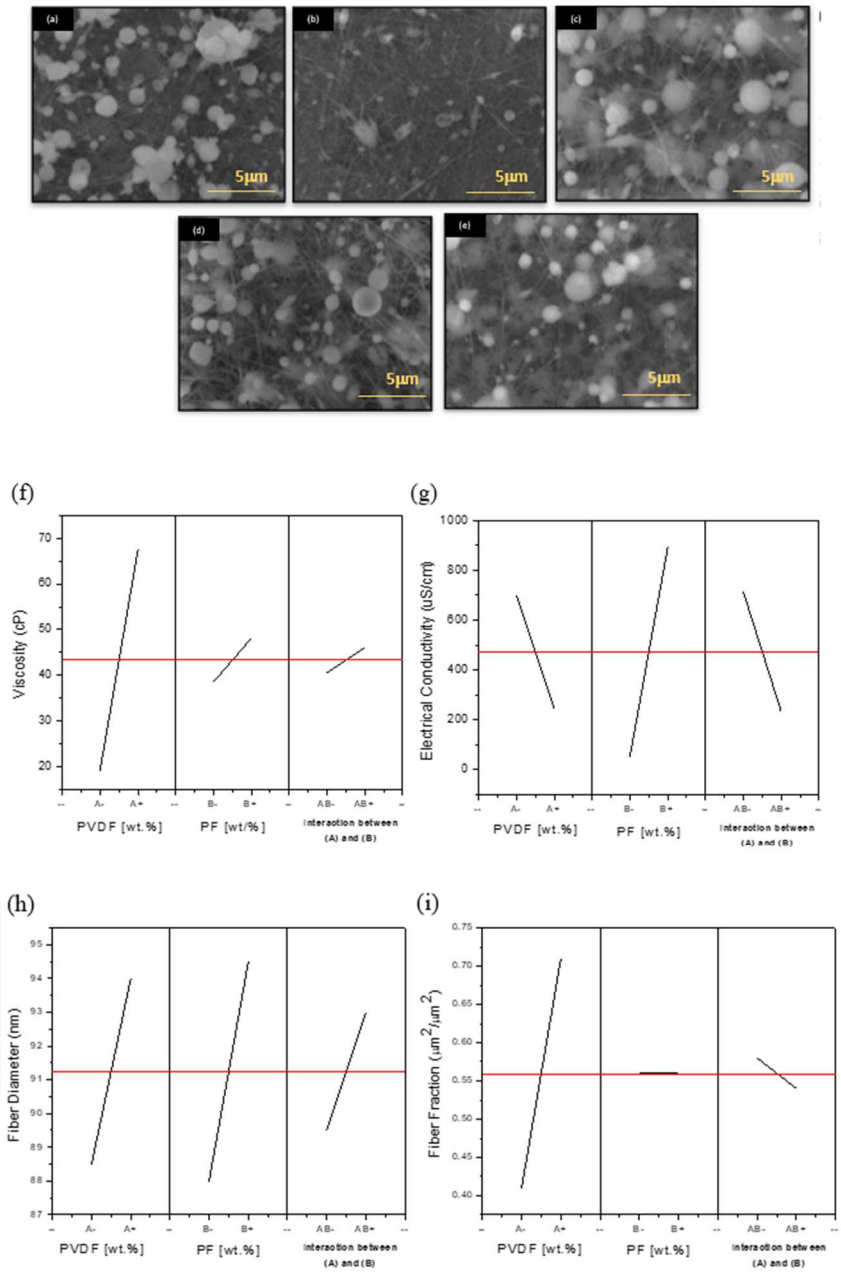

Figure 1.1 SEM images of as-spun nanofibers based on (a,b) 8 wt.% PVDF with (a) 0.5 and (b) 8.8 wt.% PF, (c) 11 wt.% PVDF, 3.0 wt.% PF and (d,e) 14 wt.% PVDF with (d) 0.5 and (e) 8.8 wt.% PF. DOE analyses showing (f) viscosity (g) electrical conductivity (h) fiber diameter and (i) fiber fraction as a function of PVDF and PF concentrations. The red solid line indicates the mean value of the respective morphology.

		Solution conditions		Solution Properties		Fiber Properties		
Sample	Code	PVDF wt.%	PVDF Mw [g/mol]	Viscosity [cP]	Electrical conductivity [μS/cm]	Average fiber diameter [nm]	Fiber fraction [$\mu m^2/\mu m^2$]	Bead density [beads/μm^2]
2.1	(- -)	14	180,000	59.9	65.17	82±24	0.72	0.28
2.2	(- +)	14	534,000	275.9	14.26	328 ± 200	0.68	0.32
2.3	(+ -)	20	180,000	200.7	47.82	455 ± 236	0.95	0.05
2.4	(+ +)	20	534,000	3767	14.73	1076 ± 593	0.75	0.25

Table 1.3 Second design of experiment matrix varying PVDF concentration and Molecular Weight (MW) each with respective low (-) and high (+) values and their effect on solution properties.

Based on these observations, second DOE was designed to further increase the fiber fraction and decrease bead density. The low (-) value for PVDF for this DOE was previous DOE's high value (+) of 14 wt.% . PF solution was kept at 0.5 wt.% for both lower and upper limit. For this DOE, Mw were altered. Previous DOE had low fiber fraction and high bead density. After intensive literature survey[23,33,34], electrospun PVDF concentrations were targeted between 14 wt.% and 20 wt.% as PVDF concentration of 25 wt.% yielded a solution too viscous to electrospin and became gel-like which was also seen during literature survey for higher PVDF concentrations[35]. . Molecular weight of PVDF was altered between 180,000 in a pellet form and 534,000 in a powdered form. From Table 1.3, it can be seen that at the same PVDF concentration, increasing the MW of the PVDF polymer have drastic effect on the viscosity of the solution. The viscosity went from 59.9 to 275.9 cP for 14 wt.% PVDF and same trend was seen for higher PVDF concentration as well.

As the viscosity of the solution increased, the average fiber diameter also increased which can be seen from Table 1.3 as well as visually in Figure 1.2a through d. Higher MW means that the length of polymer chain is longer which correlates to higher viscosity and higher average fiber diameter. The increased MW had opposite effect for the electrical conductivity. The conductivity decreased from 65.17 to 14.26 μS/cm for 14 wt.% PVDF. This resulted in decrease of fiber fraction. From DOE 1 and previous studies, it was expected that electrical conductivity effects the fiber diameter and although this was not seen in DOE 1, it is seen in DOE 2. From SEM images, it can be seen that PVDF with higher MW at the same concentration fabricated much larger average fiber diameter and less beads and clumps. As for 14 wt.% PVDF, the lower MW had more beads and clumps compared to nanofiber but at higher Mw, distinguished nanofibers can be seen. Figure 1.2e shows DOE analysis of how viscosity changed as function of PVDF concentration and MW increase of the solution. Increase in PVDF concentration and MW both had positive impact on increase in viscosity of the solution. From this, it can be predicted that increasing the PVDF concentration or MW will increase the viscosity which will also increase the average fiber diameter, which is a trend that was shown for DOE1.Figure 1.2f shows show PVDF concentration and MW have impacted the electrical conductivity of the solution. While increasing the PVDF concentration have decreased the electrical conductivity, increasing the MW predominantly decreased the electrical conductivity. From this DOE analysis, it can be concluded that increasing PVDF concentration and/or MW will decrease the electrical conductivity. Figure 1.2g supports that as the PVDF and MW increases, the fiber

diameter increased. As for fiber fraction, increasing the PVDF concentration increased fiber fraction while increasing the MW have decreased the fiber fraction. Overall, Figure 1.2h showed that combination of increased PVDF concentration and MW had negative effect on the fiber fraction. One explanation of this is that with higher MW, there was an increase in fiber diameter and decrease in bead density but because the fibers were so large, there were less fibers present per layer that showed up on the SEM images that led to slightly lower fiber fraction. The solution with higher MW did have higher viscosity and therefore resulted in bigger fiber diameter and it followed the general trend of increasing viscosity correlates with increase in fiber diameter. From DOE 2, it could be concluded that the higher MW can be used to fabricate PVDF nanofibers with bigger average fiber diameter at much lower PVDF concentration without the solution solidifying at room temperature. Overall, altering the Mw did not affect the general trend of increase in viscosity resulting in increase in fiber diameter and was independent from fiber properties.

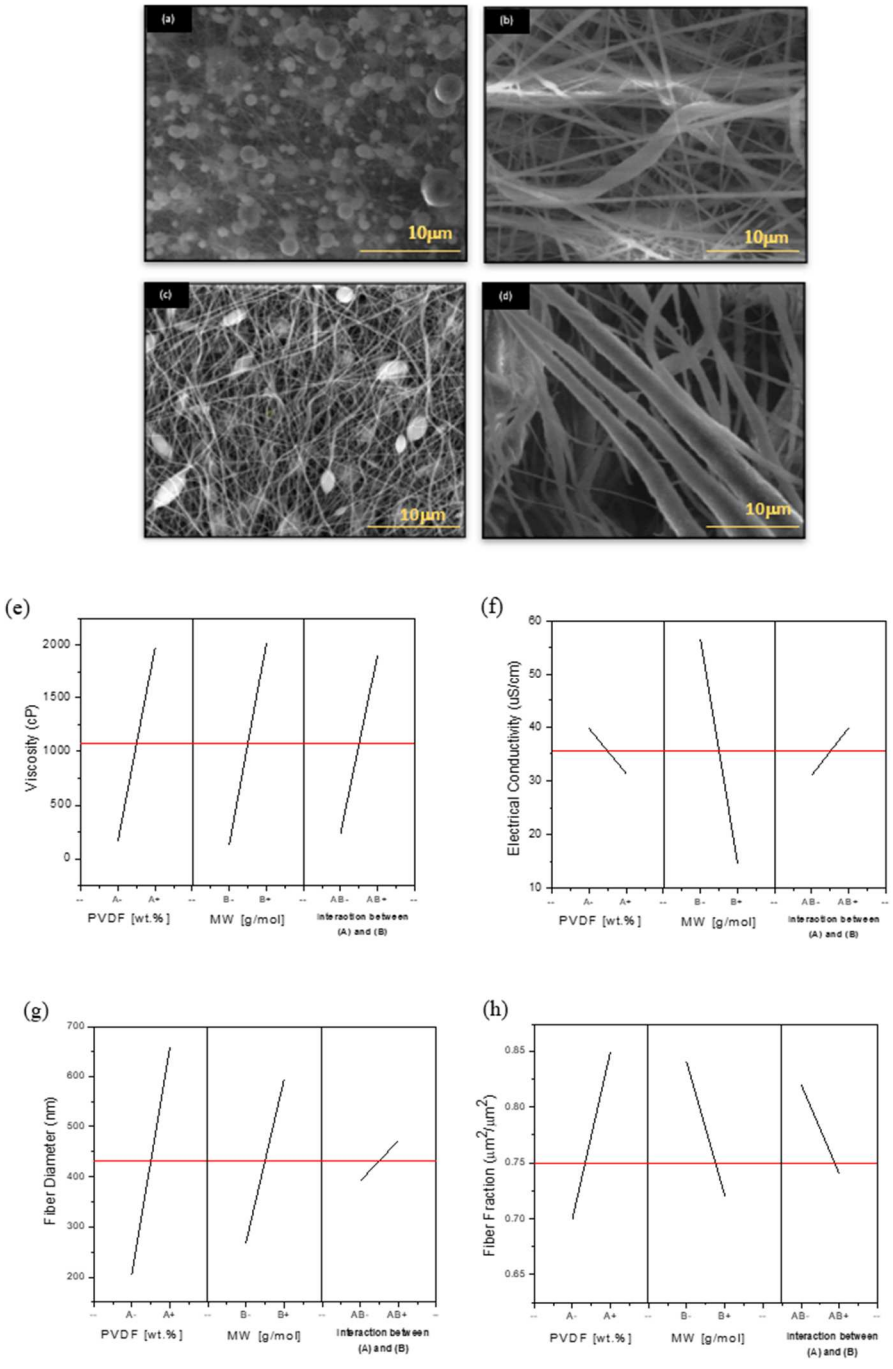

Figure 1.2 SEM images as-spun nanofibers based of (a,b) 14 wt.% PVDF with MW of (a) 180,000 (b) 534,000, and (c,d) 20 wt.% PVDF with MW of (c) 180,000 and (d) 534,000 with 0.5 wt.% PF. DOE analyses showing (e) viscosity (f) electrical conductivity (g) fiber diameter and (h) fiber fraction as a function of PVDF concentrations and MW. The red solid line indicates the mean value of the respective morphology.

From the two DOE that was conducted, Table 1.4 was created with varying PVDF wt.% and MW to create PVDF nanofiber sheet with various average fiber diameters. 0.5 wt.% PF solution was added to each solution to help increase the electrical conductivity and lower the bead density of the electrospun nanofibers. Table 1.4 shows that increasing the MW of the PVDF results in higher average fiber diameter which was the overall trend that was seen for DOE 2. Even at lower PVDF concentration, Pristine PVDF (937) had higher average fiber diameter of 937 nm at 15 wt.% compared to Pristine PVDF (455) which was at 20 wt.% PVDF but at lower MW. As expected, as the MW increased, the fiber fraction did indeed decrease as seen from DOE 2 as well. The SEM images in Figure 1.3 shows that as the Mw increased, the average fiber diameter increased as well even at a lower PVDF concentration. But as the average fiber diameter increased, the fiber fraction decreased. As the average fiber diameter increased, the number of clumps and beads decreased as well but it can be seen from SEM images that there are less amount of fibers available each layer. This explains why that Pristine PVDF (455) solution had more beads compared to other Pristine PVDF solutions but had higher fiber fraction.

	Solution conditions		Nanofiber Properties		
Sample Name	PVDF wt.%	PVDF Mw [g/mol]	Average fiber diameter [nm]	Fiber fraction [$\mu m^2/\mu m^2$]	Bead density [beads/μm^2]
Pristine PVDF (455)	20	180,000	455 ± 236	0.95	0.05
Pristine PVDF (937)	15	534,000	937 ± 491	0.89	0.11
Pristine PVDF (1021)	18	534,000	1021 ± 543	0.69	0.32

Table 1.4 Varying PVDF wt.% and molecular weight and resulting solution and nanofiber properties. 0.5 wt.% PF was added to every solution, and all electrospinning and environmental conditions were fixed at 23°C and absolute humidity of 10 g/m^3.

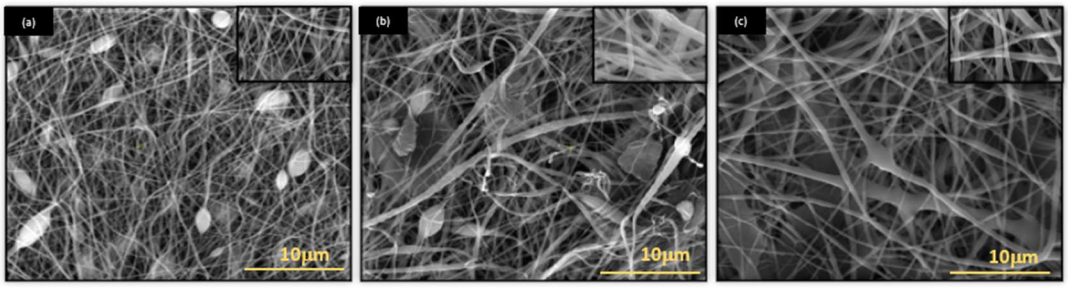

Figure 1.3 SEM images of as-spun nanofibers based on (a) 20 wt.% (b) 15 wt.% (c) 18 wt.% PVDF with 0.5 wt.% PF.

From the Table 1.4, electrospun PVDF nanofibers with average fiber diameters of 455, 937 and 1021 nm were obtained to examine how the fiber diameter effects the crystal structures of the PVDF nanofibers. FTIR spectra of PVDF nanofibers of various diameters are shown in Figure 1.4. Typically, the different conformation of PVDF is observed between 400-1500 cm^{-1} in FTIR. PVDF has 3 electroactive phases. α, β, and γ. As mentioned previously, the α-phase is non-polar and has random orientation. B-phase

has dipole moments pointing in same direction and correlates with high piezoelectric properties of PVDF. γ-phase has intermediate polar phase, and its electroactive phase is not as strong compared to β-phase. Figure 1.4 indicated α, β, and γ-phases of electrospun PVDF gathered from literature survey. The wavenumber varies slightly from literatures, so for peaks with varying wavenumber (cm^{-1}), it was carefully chosen depending on which fitted the FTIR data shown in Figure 1.4 and S1.1.[30,36–40] From Figure 1.4 it can be observed that the β phase peak at 840 cm^{-1} decreases in size as the fiber diameter increases. The α-peak at 614 cm^{-1} increased as the fiber diameter increased, and the γ-peak shown at 431 cm^{-1} is only present when the average fiber diameter is 1021nm. Even with a glance, it can be seen that the β-phase peak decreases and α-phase peak increases as the average fiber diameter increases. Gregorio et al. expected trend for post thermal treatment is that the nanofiber was annealed at 40°C, it would be mostly β-phase peak and will transform into other phases as the temperature goes up and will eventually be mostly α-phase at higher temperature.[30] When electrospun PVDF nanofibers were annealed at different temperatures as shown in Figure S1.1, it was observed that as temperature increases, the β phase peak changes shape to a longer and sharper peak which describes α or γ phases which correlates to lower piezoelectric properties when compared to a β phase.

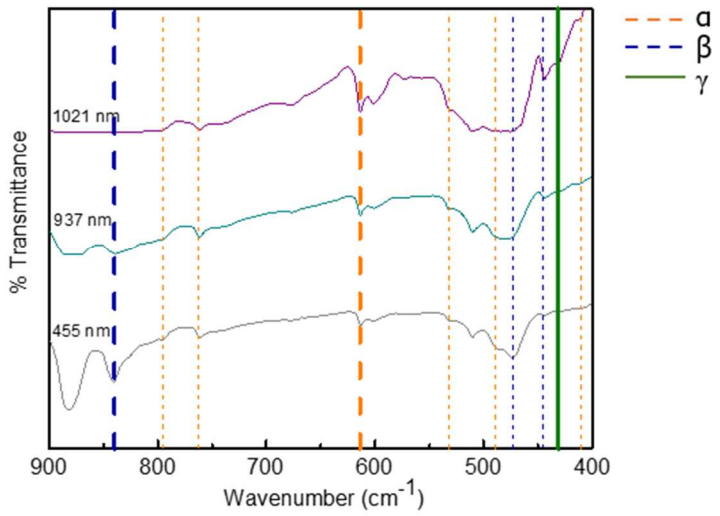

Figure 1.4 FTIR spectra of as-spun PVDF nanofibers with various average nanofiber diameters.

XRD spectra of as-spun PVDF nanofibers of various fiber diameters are shown in Figure 1.5. As the average fiber diameter increased, the β/γ peak shifted from 20.7 to 20.1°, which shows that the ratio of β phase decreased from this peak as the average fiber diameter increased and this was also shown through peak deconvolution shown in Table 1.5. Through literature survey, α, β, and γ peaks were identified in a similar way as with FTIR peaks[36–40]. Peak deconvolution was carried out by using the Origin software. Baseline was first subtracted from the of XRD patterns. Using the peaks at 18.4 and 19.9° as α-peaks, 20.1° as γ-peak and 20.7° as β-peak, the area under the curve was determined to estimate the ratio of the desired phases of PVDF. Since β-phase is correlated to the electroactive phase, Table 1.5 shows the β-phase peak ratio with corresponding average fiber diameter. This correlated with FTIR trend that as the fiber diameter decreases, the electroactive phase, β phase of PVDF increases leading to higher piezoelectric properties.

This also correlates with FTIR results of the Pristine PVDF (1021) having a very distinguishable γ-phase peak that the lower average fiber diameter PVDF solution did not have. As the as-spun PVDF nanofiber was annealed at different temperature as shown in Figure 1.6, the β peak at 20.7° shifts to the right which needs further investigation to why that is. It is more common for peaks to shift to left as it is annealed at a higher temperature due to chance in lattice parameters. Another example that supports the idea that β-peak decreases as the temperature increases is shown by the α-peak at 18.4°. This α peak maintains its shape but the peak increases slightly as the temperature increases, which supports that at high annealing temperatures, there are more α phases present for electrospun PVDF nanofibers[30]. These trends were also seen in Figure S1.2 for different average fiber diameters at different annealing temperatures as well. As the temperature increased, the β-peak at 20.7° shifted slightly to the right for all the Pristine PVDF with average fiber diameters at 455, 937 and 1021 nm. It can also be seen that the α-peak at 18.4° increases slightly as the temperature goes up.

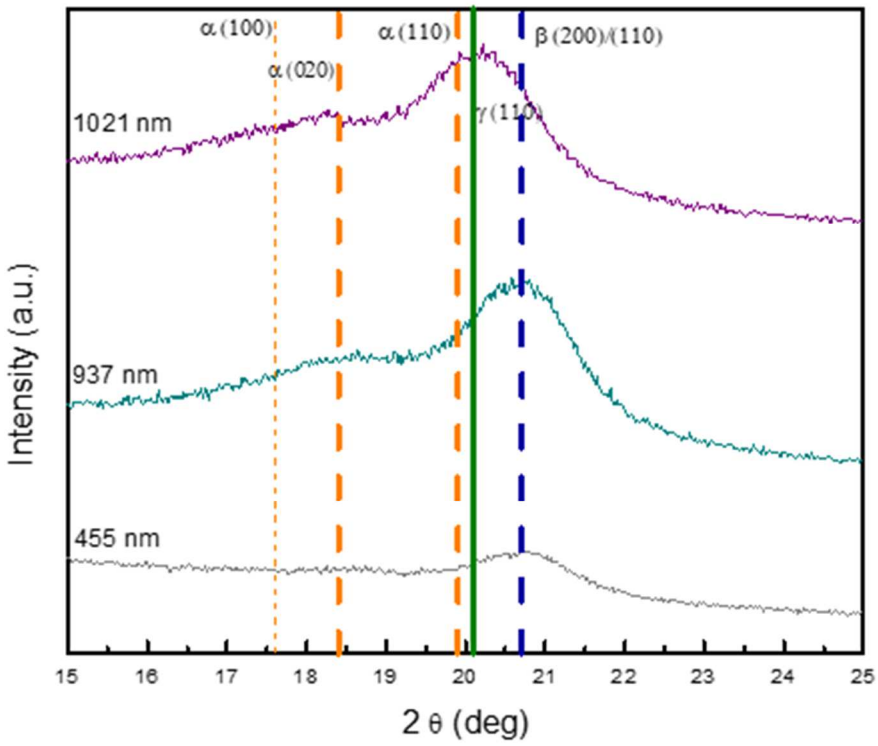

Figure 1.5 XRD spectra of as-spun PVDF nanofibers with various average nanofiber diameters.

Average fiber diameter (nm)	β/(α+β+γ) (%)
455	55
937	40
1021	37

Table 1.5 β-phase ratio based on XRD peak deconvolution of pristine PVDF nanofibers.

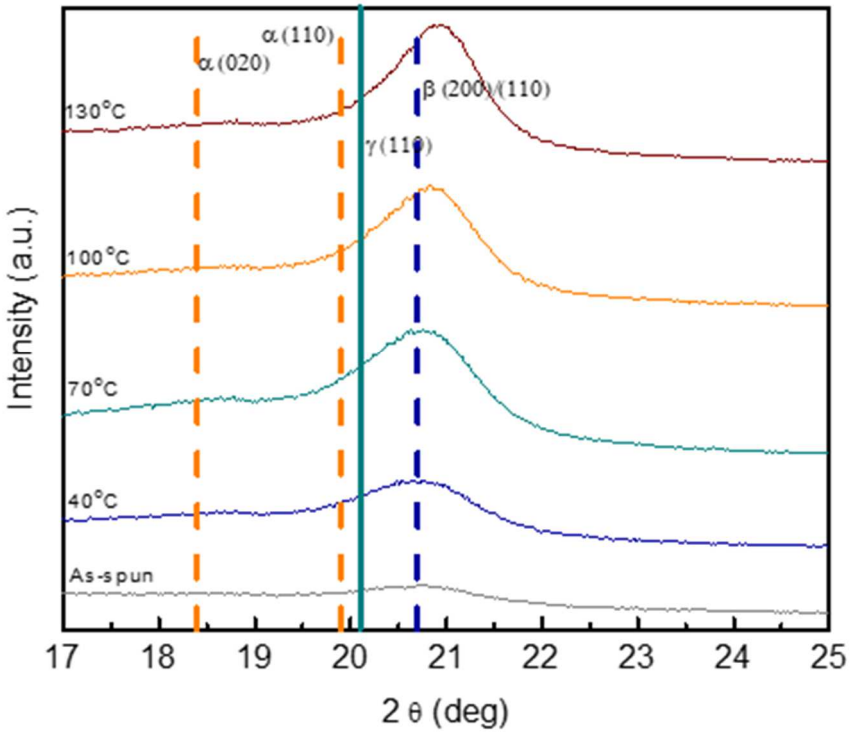

Figure 1.6 XRD spectra of PVDF nanofibers annealed at various temperatures. Average fiber diameter before annealing was 455 nm.

Annealing Temp (°C)	β/(α+β+γ) (%)
As-spun	55
40	59
70	65
100	45
130	43

Table 1.6 β-phase ratio based on XRD peak deconvolution of pristine PVDF nanofibers annealed at various temperatures. Average nanofiber diameter before annealing was 455nm.

1.4.2 Piezoelectric properties of PVDF nanofibers

Previous study[25,26,28] stated that high electric field applied during electrospinning would help with poling and stretching of PVDF polymer chains to transform the nonpolar α-phase into a polar β phase. that it has been expected that the size and temperature dependent electrospun PVDF nanofibers would further enhance the piezoelectric properties has been made before the piezoelectric properties characterizations were carried out.

Typical piezoelectric response of various PVDF nanofibers were measured in room temperature as shown in Figure 1.7a. More than triple the voltage output was observed from 32 to 106 mV as the nanofiber diameter decreased from 1021 to 455 nm, as shown in Figure 1.7b. Figure 1.7c shows the difference in voltage output at room temperature for pristine PVDF with different average fiber diameters. The red data represents Pristine PVDF (1021) and black data represents Pristine PVDF (455) and Pristine PVDF (455) has much higher output per strain compared to higher average fiber diameter. This was an expected trend for PVDF-TrFE had a similar result by Gerardo Ico for the increased order of microstructure oh polymer chains likely contributed to the enhanced piezoelectric property.[32] The trend for annealing temperature carries on to piezoelectric properties. As shown in Figure 1.7d, as the temperature increases, the voltage output decreases from 106 to 72 mV, similar as the trend that was seen for FTIR and XRD data. As the annealing temperature increases, the β phase changes to α and γ phase, thus has a slightly lower voltage output compared to electrospun PVDF nanofiber which contains more β phase[28].

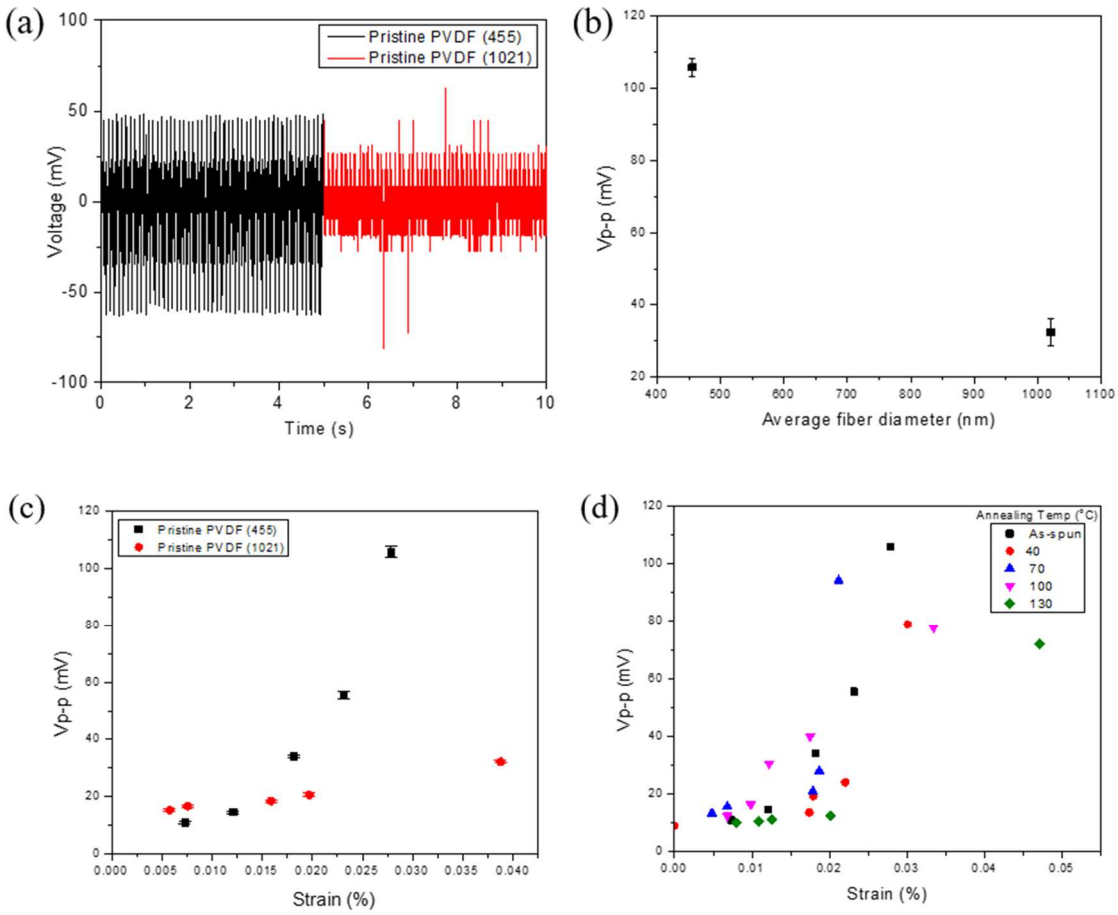

Figure 1.7 (a) Peak-to-peak voltage generation of as-spun PVDF nanofibers at average fiber diameters (b) Average peak-to-peak voltage output of as-spun PVDF nanofibers as function of fiber diameter (c) Average peak-to-peak voltage of as-spun PVDF nanofibers as a function of applied strain at 10 Hz (d) Average peak-to-peak voltage of PVDF nanofibers as a function of annealing temperature. Average diameter of as-spun nanofibers (i.e. before annealing) were 544nm.

The piezoelectric coefficient, d_{33}, was calculated using the values obtained via PFM. Figure 1.8b shows d_{33} as a function of fiber diameter. The expected trend was that as the fiber diameter decreased to below 90nm the piezoelectric coefficient will increase significantly but will remain in similar range if the fiber diameter above 100nm for PVDF-TrFE. However, the dipole orientation of the PVDF and PVDF-TrFE varies and

therefore, cannot be used as a direct comparison.[41]This trend was not seen during the experiment because the average fiber diameter was much greater than 90nm This particular trend was not seen for the range of PVDF tested because the low PVDF concentration that resulted in low average fiber diameter had too high of bead density to be able to test for piezoelectric coefficient through PFM. Further research would be required to see if d_{33} would significantly increase for PVDF for fiber diameters under 90nm. The sample that had fiber diameter of 544nm were also annealed at different temperatures to see if it follows same trend as the cantilever results. As shown in Figure 1.8c, the d33 increased slightly at 40°C and decreased as the temperature continued to increase. At 130°C, it can be seen from FTIR and XRD result that it has the smallest β-phase which is what was expected.

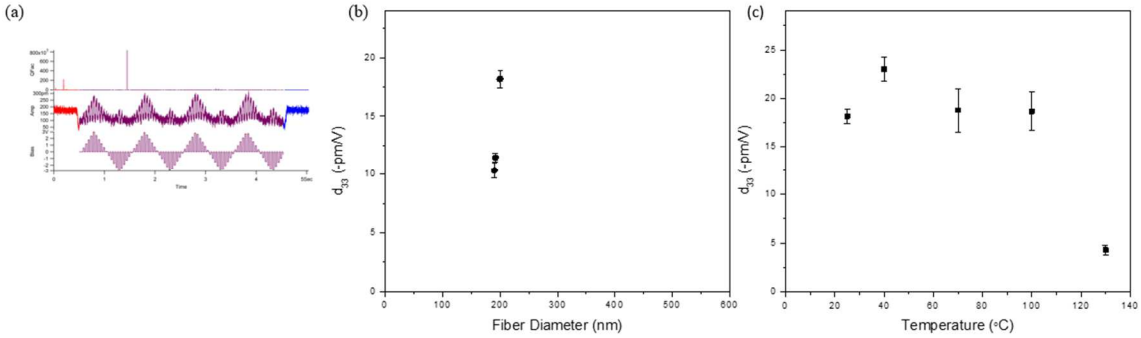

Figure 1.8 Piezoelectric force microscopy (PFM) on electrospun individual PVDF nanofibers. (a) Amplitude and bias change over time. (b) Piezoelectric charge constant (d_{33}) as a function of average fiber diameter. (c) Piezoelectric charge constant (d_{33}) as a function of annealing temperature. Fiber diameter of as-spun nanofibers (i.e. before annealing) were 544nm.

1.5 Conclusion

As-spun PVDF nanofibers were fabricated for detailed study of size and temperature dependent piezoelectric properties. Similar to other piezoelectric polymers like PVDF-TrFE and PAN, the voltage output (V_3) and piezoelectric charge constant (d_{33}) increased as the fiber diameter decreased. However, unlike PVDF-TrFE and PAN, it was shown that at higher annealing temperatures, the V_3 and d_{33} decreased for PVDF because the β-phase was transformed into another phases such as α and γ-phases. Similar result from cantilever and PFM measurement were also observed in FTIR and XRD that smaller fiber diameter had larger β-phase and the phase decrease or shifts into another phase as the annealing temperature went up. Testing electrospun PVDF nanofibers with smaller diameter would provide a better understanding and show the difference in piezoelectric properties characteristics. Results obtained from optimizing piezoelectric voltage output from this work by fabricating size and temperature dependent electrospun PVDF nanofiber has potential to be used in applications such as air filtration for reusable Personal Protective Equipment (PPE). These piezoelectric electrospun nanofiber sheet will be able to convert the mechanical stress from movements cause by breathing into electrical energy and self-charging the electrostatic media to continue to attract airborne particles without the need of recharging the filter. The electrostatic charge will not only attract the particles but with high enough voltage generated from optimization of electrospun piezoelectric nanofiber sheet, there is a potential to even rupture the bacteria or virus, making the mask reusable.

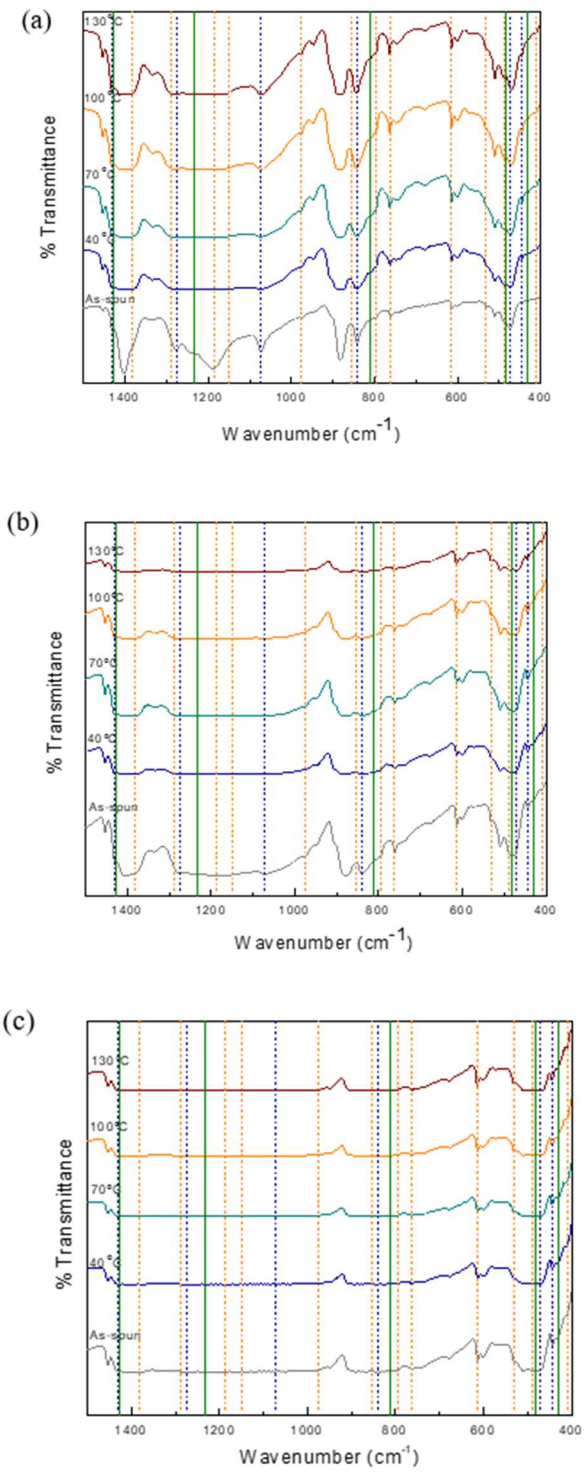

Figure S1.1 FTIR spectra of PVDF nanofibers after annealing at various temperatures. Average diameter of as-spun nanofibers (i.e. before annealing) were (a) 455 nm (b) 937 nm (c) 1021 nm.

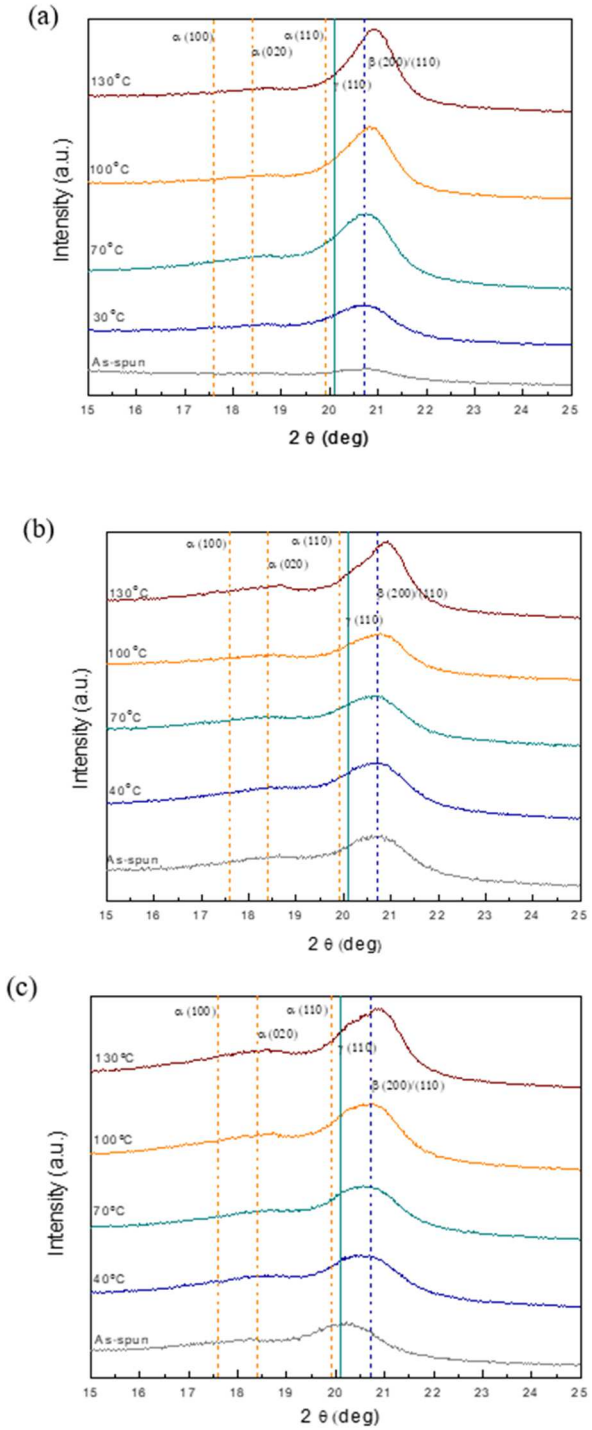

Figure S1.2. XRD spectra of PVDF nanofibers after annealing at various temperatures. Average diameter of as spun nanofibers (i.e. before annealing) were (a) 455 nm (b) 937 nm (c) 1021 nm.

1.6 References

1. Zhou, Y., Huang, W., Liu, J., Zhu, X. & Yan, D. Self-assembly of hyperbranched polymers and its biomedical applications. *Advanced Materials* vol. 22 4567–4590 (2010).

2. Encyclopedia of Tissue Engineering and Regenerative Medicine | ScienceDirect. https://www.sciencedirect.com/referencework/9780128137000/encyclopedia-of-tissue-engineering-and-regenerative-medicine.

3. Lloyd, D. R., Kinzer, K. E. & Tseng, H. S. Microporous membrane formation via thermally induced phase separation. I. Solid-liquid phase separation. *J. Memb. Sci.* **52**, 239–261 (1990).

4. Early, P. An Innovative Development Towards The Industrialization of Electrospinning Process - Hybrid Electrospinning Technology. (1964).

5. Jia, Y. T. *et al.* Fabrication and characterization of poly (vinyl alcohol)/chitosan blend nanofibers produced by electrospinning method. *Carbohydr. Polym.* **67**, 403–409 (2007).

6. Medeiros, E. S., Glenn, G. M., Klamczynski, A. P., Orts, W. J. & Mattoso, L. H. C. Solution blow spinning: A new method to produce micro- and nanofibers from polymer solutions. *J. Appl. Polym. Sci.* **113**, 2322–2330 (2009).

7. Sehaqui, H. *et al.* Cellulose nanofiber orientation in nanopaper and nanocomposites by cold drawing. *ACS Appl. Mater. Interfaces* **4**, 1043–1049 (2012).

8. Bajáková, J., Chaloupek, J., Lukáš, D. & Lacarin, M. *'DRAWING'-THE PRODUCTION OF INDIVIDUAL NANOFIBERS BY EXPERIMENTAL METHOD*. (2011).

9. Zamwar, P. *et al. A review on synthesis, advantages and disadvantages of Nanofibers*.

10. Gasparac, R., Kohli, P., Mota, M. O., Trofin, L. & Martin, C. R. Template synthesis of nano test tubes. *Nano Lett.* **4**, 513–516 (2004).

11. Tao, S. L. & Desai, T. A. Aligned arrays of biodegradable poly(ε-caprolactone) nanowires and nanofibers by template synthesis. *Nano Lett.* **7**, 1463–1468 (2007).

12. Zhang, X. & Lu, Y. Centrifugal spinning: An alternative approach to fabricate

nanofibers at high speed and low cost. *Polym. Rev.* **54**, 677–701 (2014).

13. Kenry & Lim, C. T. Nanofiber technology: current status and emerging developments. *Prog. Polym. Sci.* **70**, 1–17 (2017).

14. Hromadka, M. *et al.* Nanofiber applications for burn care. *Journal of Burn Care and Research* vol. 29 695–703 (2008).

15. Gibson, P. & Lee, C. Application of nanofiber technology to nonwoven thermal insulation. in *Proceedings of 14th Annual International TANDEC Nonwovens Conference* 1–14 (SAGE PublicationsSage UK: London, England, 2004). doi:10.1177/155892500700200204.

16. T. M., S. *et al.* A review of recent progress in polymeric electrospun nanofiber membranes in addressing safe water global issues. *RSC Adv.* **11**, 9638–9663 (2021).

17. Ma, H., Chu, B. & Hsiao, B. S. Functional nanofibers for water purification. in *Functional Nanofibers and their Applications* 331–370 (Elsevier, 2012). doi:10.1533/9780857095640.2.331.

18. Liang, W. *et al.* Transparent Polyurethane Nanofiber Air Filter for High-Efficiency PM2.5 Capture. *Nanoscale Res. Lett.* **14**, 1–9 (2019).

19. Zhang, B., Kang, F., Tarascon, J. M. & Kim, J. K. Recent advances in electrospun carbon nanofibers and their application in electrochemical energy storage. *Progress in Materials Science* vol. 76 319–380 (2016).

20. Shung, K. K., Cannata, J. M. & Zhou, Q. F. Piezoelectric materials for high frequency medical imaging applications: A review. doi:10.1007/s10832-007-9044-3.

21. Anwar, S. *et al.* Piezoelectric Nylon-11 Fibers for Electronic Textiles, Energy Harvesting and Sensing. *Adv. Funct. Mater.* **31**, 1–8 (2021).

22. Chen, H. J. *et al.* Investigation of PVDF-TrFE composite with nanofillers for sensitivity improvement. *Sensors Actuators, A Phys.* **245**, 135–139 (2016).

23. Choi, S. W., Kim, J. R., Ahn, Y. R., Jo, S. M. & Cairns, E. J. Characterization of electrospun PVdF fiber-based polymer electrolytes. *Chem. Mater.* **19**, 104–115 (2007).

24. Davis, G. T., McKinney, J. E., Broadhurst, M. G. & Roth, S. C. Electric-field-induced phase changes in poly(vinylidene fluoride). *J. Appl. Phys.* **49**, 4998–5002

(1978).

25. Wang, W. *et al.* Unexpectedly high piezoelectricity of electrospun polyacrylonitrile nanofiber membranes. *Nano Energy* **56**, 588–594 (2019).

26. Ribeiro, C., Sencadas, V., Ribelles, J. L. G. & Lanceros-Méndez, S. Influence of processing conditions on polymorphism and nanofiber morphology of electroactive poly(vinylidene fluoride) electrospun membranes. *Soft Mater.* **8**, 274–287 (2010).

27. Zheng, J., He, A., Li, J. & Han, C. C. Polymorphism control of poly(vinylidene fluoride) through electrospinning. *Macromol. Rapid Commun.* **28**, 2159–2162 (2007).

28. Yee, W. A., Kotaki, M., Liu, Y. & Lu, X. Morphology, polymorphism behavior and molecular orientation of electrospun poly(vinylidene fluoride) fibers. *Polymer (Guildf).* **48**, 512–521 (2007).

29. Motamedi, A. S., Mirzadeh, H., Hajiesmaeilbaigi, F., Bagheri-Khoulenjani, S. & Shokrgozar, M. Effect of electrospinning parameters on morphological properties of PVDF nanofibrous scaffolds. *Prog. Biomater.* **6**, 113–123 (2017).

30. Gregorio, R. & Ueno, E. M. Effect of crystalline phase, orientation and temperature on the dielectric properties of poly (vinylidene fluoride) (PVDF). *J. Mater. Sci.* **34**, 4489–4500 (1999).

31. Yu, S. & Myung, N. V. Minimizing the Diameter of Electrospun Polyacrylonitrile (PAN) Nanofibers by Design of Experiments for Electrochemical Application. *Electroanalysis* **30**, 2330–2338 (2018).

32. Ico, G. *et al.* Size-dependent piezoelectric and mechanical properties of electrospun P(VDF-TrFE) nanofibers for enhanced energy harvesting. *J. Mater. Chem. A* **4**, 2293–2304 (2016).

33. Kim, Y. J., Ahn, C. H., Lee, M. B. & Choi, M. S. Characteristics of electrospun PVDF/SiO2 composite nanofiber membranes as polymer electrolyte. *Mater. Chem. Phys.* **127**, 137–142 (2011).

34. Gao, K., Hu, X., Dai, C. & Yi, T. Crystal structures of electrospun PVDF membranes and its separator application for rechargeable lithium metal cells. *Mater. Sci. Eng. B Solid-State Mater. Adv. Technol.* **131**, 100–105 (2006).

35. Voice, A. M. *et al.* Thermoreversible polymer gel electrolytes. *Polymer (Guildf).* **35**, 3363–3372 (1994).

36. Anousheh, N., Godey, F. & Soldera, A. Unveiling the impact of regioisomerism defects in the glass transition temperature of PVDF by the mean of the activation energy. *J. Polym. Sci. Part A Polym. Chem.* **55**, 419–426 (2017).

37. Satapathy, S., Pawar, S., Gupta, P. K. & RVarma, K. B. Effect of annealing on phase transition in poly(vinylidene fluoride) films prepared using polar solvent. *Bull. Mater. Sci.* **34**, 727–733 (2011).

38. Satthiyaraju, M. & Ramesh, T. Effect of annealing treatment on PVDF nanofibers for mechanical energy harvesting applications. *Mater. Res. Express* **6**, (2019).

39. Bhatti, I. N. Effect of Annealing and Time of Crystallization on Structural and Optical Properties of PVDF Thin Film Using Acetone as Solvent. *IOSR J. Appl. Phys.* **4**, 42–47 (2013).

40. Cai, X., Lei, T., Sun, D. & Lin, L. A critical analysis of the α, β and γ phases in poly(vinylidene fluoride) using FTIR. *RSC Adv.* **7**, 15382–15389 (2017).

41. Ico, G. *et al.* Size-dependent piezoelectric and mechanical properties of electrospun P(VDF-TrFE) nanofibers for enhanced energy harvesting. *J. Mater. Chem. A* **4**, 2293–2304 (2016).

2. Antimicrobial Functionality Embedded Electrospun PVDF Nanofibers for Air Filtration Application

2.1 Abstract

With the global pandemic, the demand for personal protective equipment (PPE) such as face masks is higher than ever. N95 masks are considered the gold standard PPE against the viral pathogens and have thus suffered a shortage many times throughout the pandemic. In addition, the electrostatic charge inserted into the melt-blown polypropylene fiber-based mask material to capture bacterial and viral particles is easily removed during the disinfection process, allowing for only single use. Thus, creative solutions to enhance the reusability while exhibiting comparable protection efficiency to the N95 masks are highly desirable.

Piezoelectric polymers, which can generate electricity under mechanical strain, are emerging as an alternative face mask material to potentially "electrocute" the viral and bacterial particles as it is deformed via breathing. Electrospinning not only is a simple, cost-effective, scalable method to fabricate polymer nanofibers, but also allows for fine tuning of process conditions, enabling precise control of nanofiber properties such as morphology, which has recently been shown to significantly affect piezoelectric properties.

The overarching goal of this project is to fabricate multifunctional composite nanofibers with air filtration and antimicrobial capabilities enabled by piezoelectric effect. Diameter of PVDF nanofibers with various antimicrobial additives (e.g., silver)

function was optimized via process control of electrospinning and was correlated with piezoelectric properties characterized by cantilever testing and piezo force microscopy. Additionally, antimicrobial and exhalation and inhalation resistance are characterized and compared to the N95 mask performance. By introducing piezoelectric materials, the composite nanofibers produced with a relatively facile method could provide a reusable, high-performance, multifunctional breathing mask.

2.2 Introduction

Newly identified coronavirus called SARS-CoV-2 emerged from China in December 2019 and have caused a worldwide pandemic of respiratory illness known as COVID-19. Covid-19 virus has a round or elliptic and often pleomorphic form with a diameter approximately 60-140 nm with a crown-like appearance due to presence of spike glycoproteins on the envelope. The virus enters the body through respiratory organs and eyes. Daily number of new infections were more than 223,607 just in the United States amongst those that have symptoms and daily death specific to Covid-19 were more than 4,295. Because its form of transmission is through a close contact (within 6ft or 1.8 meters) between infected individual's bodily fluid or secretion, one of the most critical prevention methods was usage of face masks, along with frequent handwashing and avoiding touching eyes, nose, and mouth. Covid is still among us and lasted over 1.5 years. There was a point where there was a shortage of toilet papers, cleaning wipes, bleach, food, and most importantly, personal protective equipment (PPE)[1]. PPE is worn as a barrier to minimize exposure to a variety of hazards in forms of chemical, radiological, physical, electrical, etc[2]. Due to unprecedentedly high and prolonged

demand, face masks such as filtering facepiece respirator (FFR) were in shortage, and many tried to disinfect and de-contaminate masks in an attempt to reuse the FFR[1]. But this was not recommended by Centers of Disease Control and Prevention (CDC) for they were not able to consider these four key aspects to maintain the filtering efficiency of FFRs: 1. successfully inactivate the target organism; 2. does not damage the respirator's filtration; 3. does not affect the respirator's fit; and 4. be safe for the person wearing the respirator.

Current gold standard for face masks is an N95 mask (by 3M), which has 3 different layers: shell by polyester, filter by polypropylene and coverweb also by polypropylene. The term N95 comes from its ability to filter at least 95% of airborne particles and bacteria and its resistance to fluid such as synthetic blood tested by the National Institute for Occupational Safety and Health (NIOSH). The N95 filter uses electrostatic attraction to capture oppositely charged particles. This process is done by injecting a strong electrostatic charge into the air filter. Even the current gold standard N95 masks has drawbacks. Some of the drawbacks are that it is hard to breathe and is not reusable.

The current N95 can only trap bacterial or viral particles using the electrostatic method. These particles will continue to exist in between the filter and to minimize the unintentional spread of the virus from reusing the masks and spreading the COVID19, these masks are suggested for one time usage. Covid-19 virus, that are inactivated by heat, which slows down the replication of the virus or usage of the lipid solvents such as ether (>75%), ethanol or chlorine containing disinfectants to disrupt the lipid bilayer of

the virus. But as mentioned above, these disinfecting procedures does not maintain the filtering efficiency of FFRs. The N95 mask filter was also known as melt-blown filter because it uses melt-blown process. This process includes melting and compressing polymer at 250-300°C and is solidified onto a collector in random arrangement using a cooling air. Melt-blown is fast production with low cost, but it limited because the fiber diameter cannot be controlled via melt-blown process. Also, usage of high heat during melt-blown process causes disadvantages such as poor texture, air permeability and strength of the product. Melt-blown N95 filters also cannot be washed, deteriorates after disinfection with ethanol and uses raw material from petroleum. Electrospinning, on the other hand, has ability to control morphology, composition, and electrical conductivity, has high surface area to volume ratio, allows for material combination but the process depends on many variables such as environmental, solution, and electrospinning conditions.

2.2.1 Nanofiber as piezoelectric air filter

PVDF is a biodegradable polymer that can be electrospun to increase the electroactive β-phase. By optimizing the environmental, solution and electrospinning conditions, fabrication of piezoelectric PVDF nanofiber sheet is a simple process. These piezoelectric PVDF nanofibers with various fiber diameters can be used as an air filter[3,4] where mechanical stress applied, such as air filter moving as we breathe, can be turned into self-charging electrical energy that continues to generate electrostatic charge that can capture and hold bacteria and viruses. The piezoelectric PVDF nanofiber sheet has a potential to possibly even rupture the virus or bacteria if it can generate enough electrical

energy. Since the electrical energy is "recharged" by mechanicals stress that is applied, this would make the air filtration device, face mask, reusable, and no need for disinfection. By optimizing the average fiber diameter that is electrostatically charged, less filter media will be required, making easier to breathe with mask on. This will solve multiple drawbacks of current N95 masks of being one time usage and hard to breathe.

2.2.2 Addition of antimicrobial functionality to air filter

Metals and metal oxides have been widely known for their antimicrobial activities.[5] Some examples include Silver (Ag), iron oxide (Fe_3O_4), titanium oxide (TiO_2), copper oxide (CuO), and zinc oxide (ZnO). Most metal provide the bactericidal property through reactive oxygen species (ROS) as well as their physical appearance and metal ion releases. Some other organic nanoparticles that can kill microorganisms include chitosan, triclosan, benzoic acid, etc[6,7].

Of all these, silver has been most widely used as an effective antimicrobial agent again not only bacteria, virus but also fungi[8]. Silver have been used to disinfect medical devices, to treat burns or wounds and even water purification. With other supporting materials, Silver Acetate[9] and Silver nanoparticles[8] have been chosen as additives to add antimicrobial functionality. Combining the technology of electrospinning with additive functionality, there is a potential to create a piezoelectric PVDF nanofiber sheet with antimicrobial functionality embedded. This would give the potential to not only use the piezoelectric property to continuously recharge electrostatic media that attracts bacterial and viral particles but with enough voltage generated and antimicrobial functionality added, there would be two different methods that can kill airborne particles by rupturing

these particles. This idea of rechargeable and reusable mask with antimicrobial functionality was the motivation during the beginning of COVID where there were shortages of face masks for health care system as well as the general public.

2.3 Materials and Methods

2.3.1 Materials

Polyvinylidene fluoride (PVDF, MW=180,000 g/mol), pyridine, formic acid, and silver acetate (≥99.0%) were purchased from Sigma Aldrich. N,N-dimethylformamide (DMF) and acetone were purchased from Fisher Scientific. Silver nanoparticles (Ag, 99.9%, 80nm) was purchased from Nanostructured & Amorphous Materials, Inc. All materials were used without further treatment or purification.

2.3.2 Solution preparation

Additive embedded electrospinning solutions were prepared by mixing various amounts of PVDF in 64:36 DMF/Acetone (by vol.). For Silver Nanoparticles embedded PVDF solution, desired silver nanoparticles were placed in DMF, and water bath sonicated for 2 hours with 15 minutes rest after the first hour. Once the water bath sonication was finished, PVDF was added and vigorously stirred at approximately 70 °C until homogenous. Once the solution as cooled to room temperature, acetone was added and then stirred until homogenous. Pyridinium formate (PF) was obtained by mixing equimolar amounts of pyridine and formic acid and then was added to the PVDF solution to increase the electrical conductivity.

For silver acetate solution, start off with mixing PVDF into DMF and stir vigorously at 70°C until homogenous. Once the solution as Silver Acetate was then

added and the vial was covered with foil, or light resistant vial was used for silver acetate is sensitive to light. Once the solution looks homogenous, add PF solution that was prepared by mixing equimolar amounts of pyridine and formic acid. All solutions were allowed to reach room temperature before continuing onto the next step.

2.3.3 Electrospinning

The prepared PVDF solutions were drawn into a 5-mL BD Luer Lok syringe with a 25 or 20-guage needle, which was then loaded onto a syringe pump (New Era, NE-100). The needle tip was set at 10 cm from the drum collector. Negatively charged 16.5 kV was applied to the needle tip. The grounded drum collector was wrapped with aluminum foil and rotating at 400 rpm. Environmental conditions were kept constant at temperature of 23 °C and absolute humidity of 0.00001kg water/kg dry air.

2.3.4 Nanofiber properties characterization

Morphology of the nanofiber samples was observed with a scanning electron microscope (SEM, Fisher Scientific Prisma E). Obtained SEM images were imported to ImageJ software to measure the average fiber diameter, which was obtained by measuring the length of 30 unique nanofibers. Bead density was calculated by dividing the total number of beads from a single SEM image by the total area of the image. Fiber fraction was determined by the proportion of nanofibers in the total product, which could include beads and clumps. The molecular and crystal structure were observed with Fourier-transform infrared spectroscopy (FTIR, Perkin Elmer Frontier) and X-ray diffraction (XRD, Bruker D8 Discover), respectively. FTIR spectra were obtained by scanning from 400 to 4000 cm^{-1} at a resolution and scan increment of 2 and 0.5 cm^{-1},

respectively. Sample purity and phase analysis were evaluated using X-ray diffraction performed at room temperature using an in-house Bruker D8 Discover at $\lambda = 1.5406$ Å. Data was collected over the range of 10° - 60° in scattering angle (2θ) with a step size of 0.024°.

2.3.5 Nebulizer testing

The antimicrobial activity of AgNP-containing materials was tested using methods adapted from Huang et al[10]. The inoculum broth was produced by combining 25 mL of LB Broth (Defibro) and 60 mL of *E. coli* and was left in a shaking incubator (150 rpm) at 37º C overnight, as per EPA Methods 1602[11]. The suspension was measured at 600 nm to ensure the optical density was between 0.6 and 1. The filter fibers were cut into 1 cm by 2 cm rectangles and were uniformly placed in a mason jar. The nebulizer (Aeromist Compact Nebulizer Compressor Kit, Medline) was filled with 10 mL of inoculum broth and the discharge end of the jet nebulizer chamber was hooked to the top of the mason jar by inserting it into a drilled hole. The nebulizer ran for 20 minutes, then was turned off and droplets were allowed to settle for 10 minutes. Filter fibers were left to dry overnight.

The dry filter fibers were transferred using sterilized forceps to a microcentrifuge tube containing 1.3 mL of 1X PBS. The tubes were incubated for 1 hour at 37º C and then were vortexed for 45 seconds at 2000 rpm to remove any bacteria on the surface of the material. Serial dilutions were produced and plated in triplicate in mTEC agar plates. The plates were incubated at 37º C for 18 hours before counting for colony forming units

(CFU). Blank plates were also incubated for quality control to ensure that contamination did not occur.

2.3.6 Filter efficiency testing

The procedure described in 42 CFR 84.181 for certifying N95 Filtering Facepiece Respirators (FFRs) was followed to test the efficiency of filter media in respirators, surgical masks, and other filterable material. N95 FFRs are designed for atmospheres for which there are no (N) oil droplets present and which are >95% efficient under the established testing conditions. The testing procedure requires an NaCl aerosol generated from a 2% solution applied to a nebulizer (Model 3076, TSI Inc., Shoreview, MN). The droplet aerosol was dried by passing through a heated steel tube and then charge-neutralized with a bi-polar ion source (Model 3088, TSI Inc., St. Paul, MN). The generated aerosol was diluted with filtered air resulting in a particle-laden air at 25°C (77°F) and 35% relative humidity. Aerosol generation was started and allowed to stabilize for at least five min before testing.

The N95 efficiency test is required to be conducted given a continuous airflow of 85 L/min pulled through an entire FFR with a vacuum pump. This flow rate is equivalent to a breathing minute volume under high working exertion and is therefore a worst-case condition. However, in these tests a column (Figure 2.1) with a 27-mm diameter inner hole was used to test a portion of a surgical mask rather than the entire mask. The column is detachable so that the FFR portion could be placed between the upper and lower portions and clamped together to ensure that there were no air leaks around the filter portion. The flow rate through the column was adjusted such that the velocity of air

drawn through the column (face velocity) was the same as the face velocity of an entire FFR at 85 L/min of 8 cm/s. For these studies, the area of a 3M 8210 mask (175 cm^2) was used to represent the surgical masks tested. Airflow calibration was conducted using a primary calibrator (Gilian Gilibrator 2, Sensidyne, Clearwater, FL) before each test.

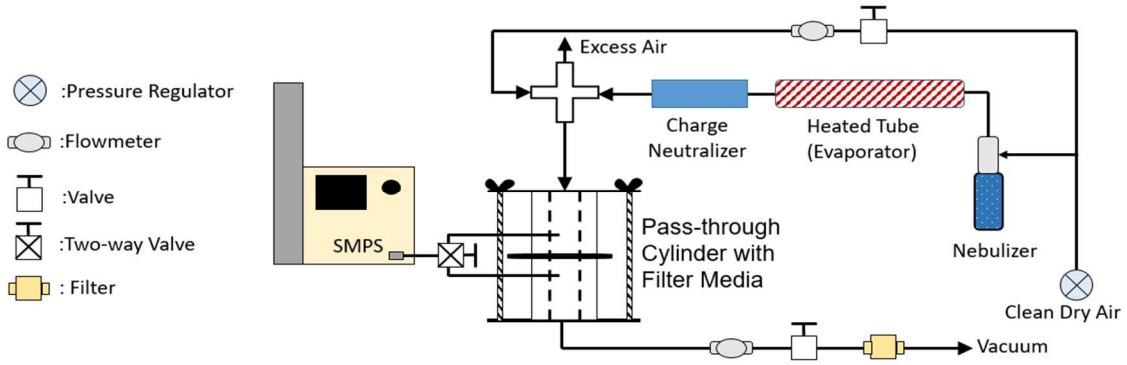

Figure 2.1 Filtering Facepiece Respirators (FFR) efficiency testing apparatus.

Aerosol particle count and size distribution were measured with a scanning mobility particle sizer (SMPS) consisting of electrostatic classifier (Model 3080, TSI Inc., Shoreview, MN) in combination with a condensation particle counter (CPC) (Model 3785, TSI Inc., Shoreview, MN). The SMPS counted particles within 103 channels ranging between 7 – 289 nm. As required by the certification procedure, the NaCl aerosol is to have a geometric mean diameter of 0.075 µm and a geometric standard deviation of 1.8, which was verified with the SMPS prior to a test. As shown in Fig. 13, the sample line to the SMPS was evenly split to enable sampling of particles upstream and downstream of the filter media held in the central portion of the sample column. A valve was manually turned to direct flow to the SMPS from the upstream side of the filter media to the downstream side. Particle efficiency was determined as a ratio of the particle

concentration downstream (C_d) of the mask sample and upstream of the (C_u) of the mask sample over the entire range of the NaCl particle distribution.

$$E(\%) = \left(1 - \frac{C_d}{C_u}\right) 100$$

The trials were conducted using the guidance in 42 CFR 84 with two exceptions. The masks were not preconditioned in an 85% RH and 37 C atmosphere for 24 hours prior. The certification method preloads the filter with up to 200 mg of salt first and then takes measurements. Here, measurements were made on "neat" filter media. Measurements made during these trials are therefore more conservative (potentially lower measured efficiency) because the preload process would increase the efficiency of filter media.

2.3.7 Filter pressure drop testing

Filter pressure drop, or "breathing resistance," measurements were conducted using the pass-through cylinder. The same ports used to sample above and below the filter media were connected to a sensitive, calibrated pressure transmitter (Series 646, Dwyer Instruments, Inc., Michigan City, MI) that measures in the range of 0 – 65 mm H_2O air pressure. NIOSH stipulates that an N95 should not exceed 30 mm H_2O when tested at 85 L/min. The voltage output signal of the transmitter was received by an analog-to-digital converter and read using the LabVIEW software system (National Instruments, Austin, TX). During a pressure trial, the media was subjected to the same flow rate applied to the mask as when determining particle capture efficiency. It should be noted that pressure drop measurements were made before efficiency measurements, so the values reflect the pressure drop of the filter media before it was doped with NaCl particles.

2.4 Results and Discussion

Silver acetate and silver nanoparticles were added to PVDF solution to introduce the antimicrobial functionality to the electrospun nanofiber sheet. Looking at Table 2.1, adding silver acetate (AgAc) and silver nanoparticles (AgNP) to 20 wt.% PVDF with 0.5 wt.% PF solution resulted in increase in diameter from 455 to 655 and 862 nm respectively. The fiber fraction also increased from 0.79 to 0.94 and 0.99 mm^2/mm^2 with AgAc and AgNP, respectively. Looking at the SEM images in Figure 2.2, There are significantly less beads and clumps present in the solution with additives embedded shown in Figure 2.2b and 2.2c. Figure 2.2b and c used backscatter electron for SEM image and the contrast is based on atomic weight. Ag is heavier compared to F (or C and H) of PVDF and therefore it showed up brighter in the image. This is evident in Figure 2.2c with brighter spots referring to the Ag that are evenly distributed amongst nanofibers. Figure 2.2b shows Silver Acetate embedded PVDF solution and some AgAc is seen due to crystalizing, but it is not as present or uniformly distributed compared to Silver Nanoparticle embedded solution. Figure 2.2d shows color SEM of AgNP embedded PVDF solution. The green represents the Ag nanoparticles and purple shows carbon and fluoride. Figure 2.2d shows very similar distribution as Figure 2.2c but with color SEM, it can be seen that there are Ag distributed among the nanofibers even where there are not distinct specs of Ag nanoparticles visibly seen.

	Solution conditions				Nanofiber Properties			
Solution Name	PVDF wt.%	PVDF Mw [g/mol]	Additive	Additive wt.%	Average fiber diameter [nm]	Standard deviation [nm]	Fiber fraction [$\mu m^2/\mu m^2$]	Bead density [beads/mm^2]
Pristine PVDF (455)	20	180,000	N/A	N/A	455	236	0.95	0.05
Pristine PVDF (937)	15	534,000	N/A	N/A	937	491	0.89	0.11
Pristine PVDF (1021)	18	534,000	N/A	N/A	1021	543	0.69	0.32
AgAc/PVDF (655)	20	180,000	AgAc	10	655	3223	0.94	0.06
AgNP/PVDF (862)	20	180,000	AgNP	6.67	862	552	0.99	0.01

Table 2.1. Pristine and additives embedded PVDF solutions. 0.5 wt.% PF was added to every solution. All electrospinning and environmental conditions were fixed at 23°C and absolute humidity of 10 g/m^3.

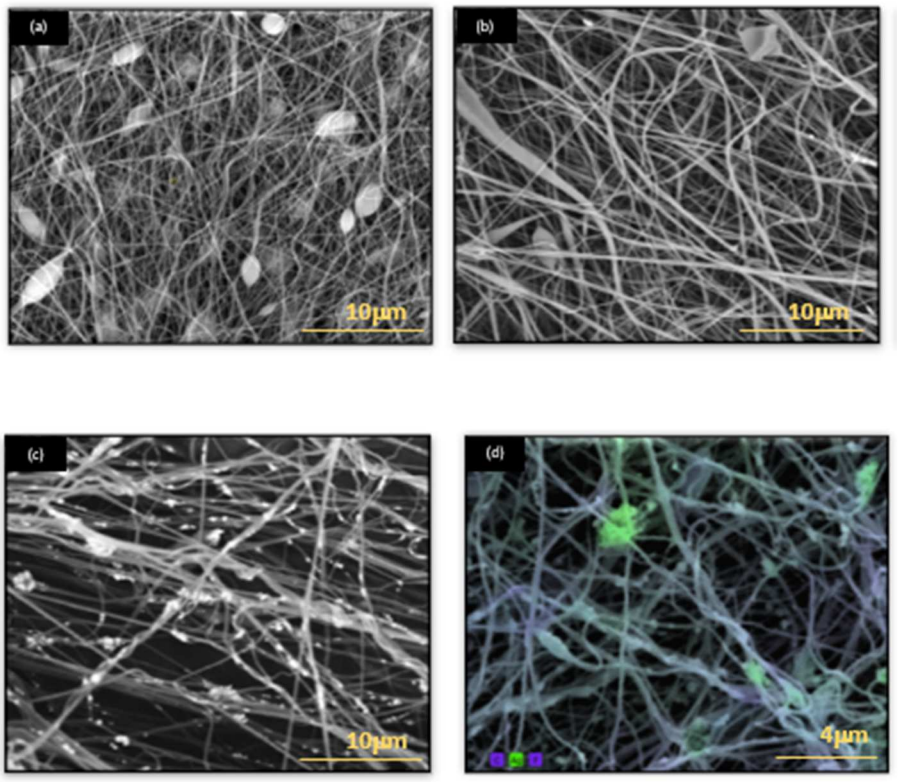

Figure 2.2 SEM images of as-spun nanofibers of (a) 20 wt.% PVDF (b) 20 wt.% PVDF, 10 wt.% AgAc (c),(d) 20 wt.% PVDF, 6.67 wt.% Ag. PF concentration was fixed at 0.5 wt.% for all samples, while electrospinning and environmental conditions were fixed at 23°C and absolute humidity of 10 g/m^3.

FTIR was run for these three solutions to see if additives would change the crystal structure of the solution. Looking at Figure 2.3, when additives were added to PVDF solution, the α, β, and γ- phases that were seen for Pristine PVDF (455) were not as evident for AgNP/PVDF (862) and AgAc/PVDF (655). AgAc added and AgNP embedded PVDF solutions did not show clear peaks of where the peaks should have been compared to few figures from other literatures.[12,13] For better result, another FTIR testing or further research would have to be conducted to find out why this was the case for the additive embedded PVDF solutions.

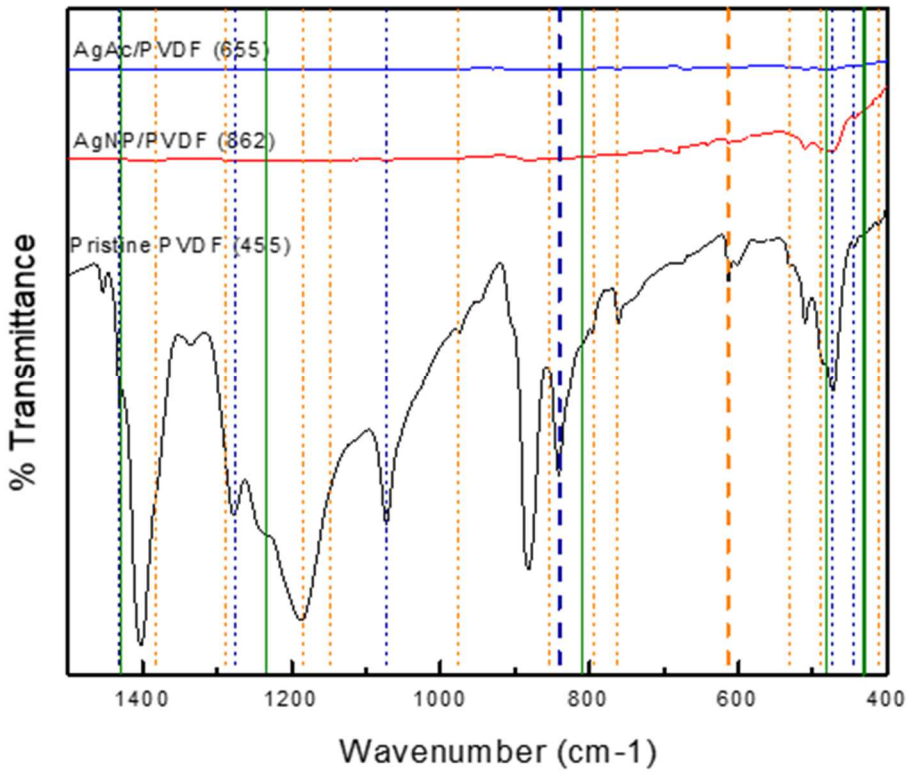

Figure 2.3 FTIR spectra of additive embedded as-spun PVDF nanofibers with various average nanofiber diameters.

The XRD results shown in Figure 2.4 was similar compared to FTIR results. The β-peak that is present at 20.7° is not present for AgNP/PVDF (862) but the peak is present where the γ-peak is at 20.1° The β-peak is present at 20.7 for AgAc/PVDF (655) but it can be seen that the peak is less evident compared to Pristine PVDF (455).[14] AgAc/PVDF (655) XRD result as has a beak at 18.3° and this is a peak that represent silver acetate[15]. Although the XRD shows a very distinctive AgAc peak, FTIR results did not show this.

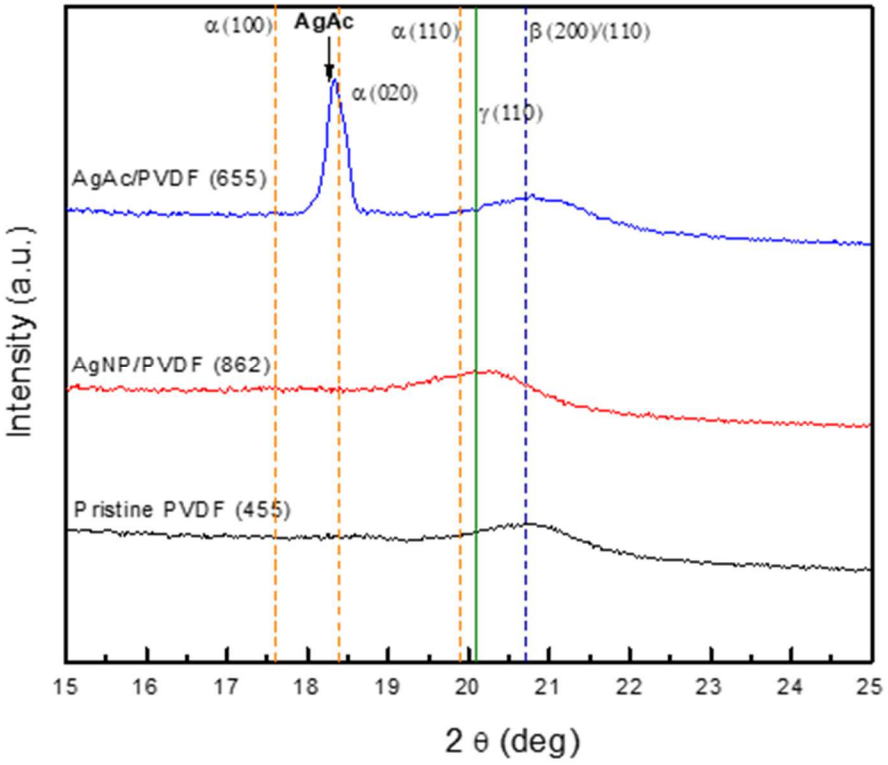

Figure 2.4 XRD spectra of additive embedded as-spun PVDF nanofibers with various average nanofiber diameters.

To see if these additive embedded PVDF solutions were suitable as a antimicrobial multifunctional air filtration system, antimicrobial testing were done on these samples. Figure 2.5a shows results of nebulizer trial with 1 hour incubation in Phosphate Buffered Saline (PBS) for various as-spun PVDF nanofibers with various fiber diameters and additives. For all the Pristine PVDF samples with average fiber diameter of 455, 937 and 1021nm, there were colonies that were formed on the samples after nebulizing. It was expected that as the fiber diameter increased, there would have been more colonies formed onto the sample due to decreased surface area, however the result was the opposite. As the fiber diameter increased, there were less colonies formed onto the sample. This would need further investigation to figure out why this have happened. The limit of detection (LOD) is 10 colony forming units (CFU) for this assay. AgNP/PVDF (862) and AgAc/PVDF (655) resulted in below LOD and had no colonies formed, showing antimicrobial functionality. Figure 2.5b shows the calculated percent removed compared to the initial E. Coli culture used in the nebulizer. The two materials that were below the limit of detection, AgNP/PVDF (862) and AgAc/PVDF (655), showed up as 100% removal but this does not mean that there was 100% removal in reality, but this was calculation based on the experimental set-up. Despite the CFU that were present for Pristine PVDFs from Figure 2.5a, the precent removal (%) were higher than 99.99% for all the as-spun PVDF solutions with different average fiber diameters. This shows that electrospun Pristine PVDF, even without antimicrobial additives, have close to 100% removal against E. coli and has great potential to be used as an air filter.

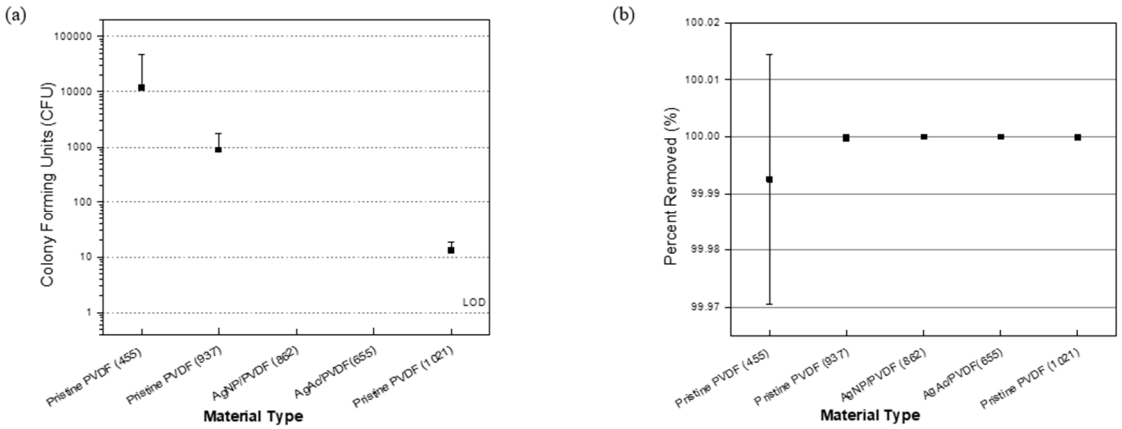

Figure 2.5 (a) Nebulizer trial with 1 hour incubation in Phosphate Buffered Saline (PBS) for electrospun PVDF with various fiber diameters and additives. (b) Percent removal calculated based on initial E. Coli broth.

To further test if these electrospun PVDF nanofiber sheets were suitable to be used as an air filter for mask application, filter efficiency testing and pressure drop testing were also conducted that can be seen in Figure 2.6. Figure 2.6a shows the filter efficiency (%) for the Pristine PVDFs with average fiber diameter 455, 937, 1021nm and additive embedded solutions, AgNP/PVDF (862) and AgAc/PVDF (655). All the samples showed excellent results of ≥ 99.8 % efficiency. Figure 2.6b shows the results for the pressure drop testing that was done for all 5 samples that were mentioned. As mentioned above, the NIOSH standard for pressure drop is 30 mm H_2O and Pristine PVDF (937), Pristine PVDF (1021) and AgNP/PVDF (862) showed pressure drop below this value. In the preliminary results, the Pristine PVDF (455) and AgAc/PVDF (655) did not meet the pressure drop standard of 30 mm H_2O, however, with precent removal and filter efficiency being far over 95%, the thickness of the samples can be further reduced to lower the pressure drop since pressure drop is directly correlated to the thickness of the sample. While the percent removal and filter efficiency testing will not be directly

correlated to the thickness of the sample, by decreasing the thickness of these samples, lower pressure drop would be able to be achieved in the future. Looking at all the data combined, Silver Nanoparticles embedded PVDF nanofibers showed the greatest potential through nebulizer trial, percent removed, filter efficiency and pressure drop testing with results being better than current N95 masks.

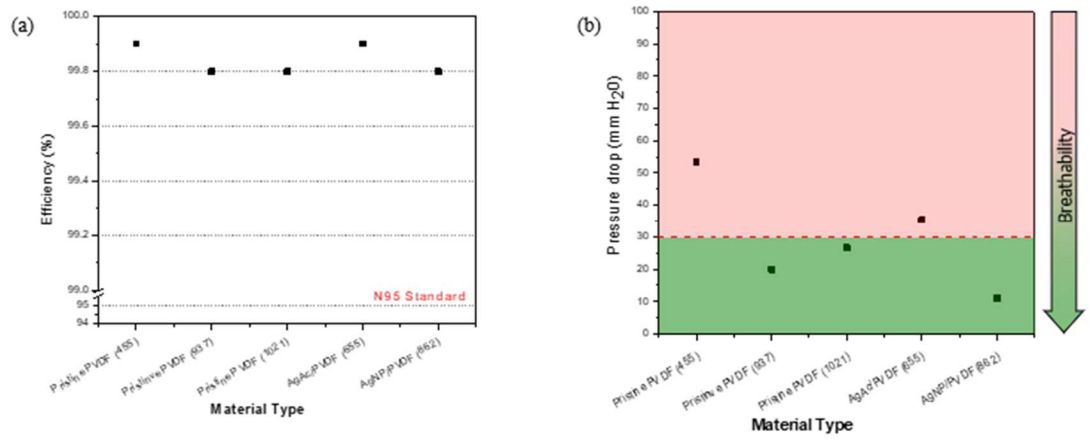

Figure 2.6 (a) Efficiency testing and (b) Pressure drop testing results for electrospun PVDF with various fiber diameters and additives.

2.5 Conclusion

Silver Acetate (AgAc) and Silver Nanoparticles (AgNP) have been known to be antimicrobial and have been used for medical applications previously. Adding these additives to electrospun piezoelectric PVDF nanofiber sheet allows to add antimicrobial functionality which is not an option for melt-blown processed filters. These additive embedded PVDF nanofibers have been tested for antimicrobial functionality, percent removal, filter efficiency, and pressure drop to see if it would have the potential to be

used as an air filter application. The results were promising for both additives as antimicrobial functionality, and Pristine PVDFs with different average fiber diameters showed colonies formed onto the sample, but when percent removal was calculated, all 5 samples that were tested had over 99.99% removal based on the tested E. coli broth. This showed that electrospun pristine PVDF is capable of 99.99% removal even without antimicrobial functionality added. Silver Nanoparticle embedded PVDF solution showed the lowest pressure drop of 11 mm H_2O, cutting the pressure drop by about 66% compared to the current N95 masks. Future research would have to be conducted to see if the AgNP/PVDF (862)'s piezoelectric properties have been maintained because the results from XRD and FTIR did not show distinct β-peak that were present for Pristine PVDF solutions. If the AgNP/PVDF (862) does have piezoelectric properties, as expected to since PVDF is a piezoelectric polymer, it would be a perfect candidate to hold the piezoelectric and antimicrobial functionality to be used as an air filter that can make masks easier to breathe, multifunctional and reusable.

2.6 Reference

1. Rubio-Romero, J. C., Pardo-Ferreira, M. del C., Torrecilla-García, J. A. & Calero-Castro, S. Disposable masks: Disinfection and sterilization for reuse, and non-certified manufacturing, in the face of shortages during the COVID-19 pandemic. *Saf. Sci.* **129**, 104830 (2020).

2. Chua, M. H. *et al.* Face Masks in the New COVID-19 Normal: Materials, Testing, and Perspectives. *Research* **2020**, 1–40 (2020).

3. Nanofiber filter media for engine air intake filtration. https://www.mann-hummel.com/en/insights/research-development/filter-technology/nanofiber-filter-media-for-engine-air-intake-filtration.html.

4. Liang, W. *et al.* Transparent Polyurethane Nanofiber Air Filter for High-Efficiency PM2.5 Capture. *Nanoscale Res. Lett.* **14**, 1–9 (2019).

5. Loomba, L. & Scarabelli, T. Metallic nanoparticles and their medicinal potential. Part I: Gold and silver colloids. *Therapeutic Delivery* vol. 4 859–873 (2013).

6. Beyth, N., Houri-Haddad, Y., Domb, A., Khan, W. & Hazan, R. Alternative antimicrobial approach: Nano-antimicrobial materials. *Evidence-based Complementary and Alternative Medicine* vol. 2015 (2015).

7. Gao, Y., Truong, Y. B., Zhu, Y. & Louis Kyratzis, I. Electrospun antibacterial nanofibers: Production, activity, and in vivo applications. *Journal of Applied Polymer Science* vol. 131 9041–9053 (2014).

8. Rai, M., Yadav, A. & Gade, A. Silver nanoparticles as a new generation of antimicrobials. *Biotechnology Advances* vol. 27 76–83 (2009).

9. Hindi, K. M. *et al.* Synthesis, stability, and antimicrobial studies of electronically tuned silver acetate N-heterocyclic carbenes. *J. Med. Chem.* **51**, 1577–1583 (2008).

10. Huang, L. *et al.* Self-Reporting and Photothermally Enhanced Rapid Bacterial Killing on a Laser-Induced Graphene Mask. *ACS Nano* **14**, 12045–12053 (2020).

11. of Science, O. Method 1602: Male-specific (F +) and Somatic Coliphage in Water by Single Agar Layer (SAL) Procedure. (2001).

12. Issa, A., Al-Maadeed, M., Luyt, A., Ponnamma, D. & Hassan, M. Physico-Mechanical, Dielectric, and Piezoelectric Properties of PVDF Electrospun Mats

Containing Silver Nanoparticles. *C* **3**, 30 (2017).

13. Seyhan, M. *et al.* Interfacial surfactant competition and its impact on poly(Ethylene oxide)/Au and poly(ethylene oxide)/Ag nanocomposite properties. *Nanotechnol. Sci. Appl.* **10**, 69–77 (2017).

14. Gregorio, R. & Ueno, E. M. Effect of crystalline phase, orientation and temperature on the dielectric properties of poly (vinylidene fluoride) (PVDF). *J. Mater. Sci.* **34**, 4489–4500 (1999).

15. Siddiqui, M. R. H., Alshehri, S., Warad, I. K., Abd El-Salam, N. M. & Mahfouz, R. M. Model free approach for non-isothermal decomposition of un-Irradiated and γ-irradiated silver acetate: New route for synthesis of Ag2O Nanoparticles. *Int. J. Mol. Sci.* **11**, 3600–3609 (2010).

3. Summary and Perspective

The aim of this work was to study enhancement of piezoelectric properties of polyvinylidene fluoride (PVDF) nanofibers by electrospinning and post thermal treatment. By optimizing solution, environmental, electrospinning conditions during the process of electrospinning a solution, the molecules were aligned along the nanofiber and α-phase were transformed into β-phase. Design of Experiment (DOE) was used to precisely control the solution concentration to come up with a recipe with various fiber diameter and high fiber fraction with lower number of beads and clump present in electrospun nanofibers. This was further enhanced using post thermal treatment where increase in β-phase were seen for temperature between 40-70°C.

The concept of antimicrobial functionality embedded electrospun PVDF nanofibers for antimicrobial mask was tested in Chapter 2. Once pristine PVDF with various average fiber diameters were produced, silver nanoparticles and silver acetates were added to pristine PVDF to make composite PVDF to add antimicrobial functionality. These various nanofibers were then tested for antimicrobial ability, bacterial filtration efficiency and pressure drop to compare to the current gold standard, N95 mask.

Looking ahead, further decreasing the average fiber diameter of electrospun PVDF will be beneficial in investigating how the piezoelectric properties changes as function of nanofiber dimensions and crystallinity. Further testing to see if AgNP and AgAc embedded composite PVDF NF show piezoelectric properties through cantilever and PFM testing and see how long these materials can generate piezoelectricity to also

test for the reusability of these materials. The thickness of the electrospun NF can be altered to see how it correlates with the pressure drop and how this may also alter the result of bacterial efficiency testing. Other testing such as Viral Filtration Efficiency (VFE) testing, hydrophobic and hydrophilic tests can be done on pristine and composite PVDF solutions to further compare these materials to current N95 filter.